1 ***Tracing sulfate recycling in the hypersaline Pétrola Lake (SE Spain): A***

2 ***combined isotopic and microbiological approach***

3 N. Valiente[a], R. Carrey[b], N. Otero[b,c], M.A. Gutiérrez-Villanueva[a], A. Soler[b], D. Sanz[a], S.

4 Castaño[a], and J.J. Gómez-Alday[a]

5 **a** Biotechnology and Natural Resources Section, Institute for Regional Development

6 (IDR), University of Castilla–La Mancha (UCLM), Campus Universitario s/n, 02071

7 Albacete, Spain

8 **b** Grup d'Mineralogia Aplicada i Medi Ambient, Dep. Mineralogia, Petrologia i Geologia

9 Aplicada, Facultat de Ciències de la Terra, Universitat de Barcelona (UB), C/ Martí i

10 Franquès s/n, 08028, Barcelona, Spain

11 **c** Serra Hunter Fellowship, Generalitat de Catalunya, Spain
12

13 ***Abstract***

14 Sulfur (S) plays a significant role in saline environments, and sulfate (SO_4^{2-}) is

15 an important component of the biogeochemical S-cycle since it acts as the main

16 electron acceptor in anoxic sediments. The purpose of this paper is to evaluate

17 the fate of S, its origin, and processes affecting sulfate outcome in the

18 hypersaline Pétrola Lake in the Castilla-La Mancha region (High Segura Basin,

19 SE Spain). The lake is the terminal discharge zone of an endorheic basin with

20 considerable anthropogenic pressures. Anthropogenic activities (mainly

21 agricultural inputs and wastewater discharge), together with bedrock leaching of

22 sulfate and sulfide-rich sediments, increase dissolved SO_4^{2-} in surface and

23 groundwater up to 123,000 mg/L. The source and fate of sulfate in this

24 environment was investigated coupling hydrochemistry, including hydrogen

25 sulfide (H_2S) microprofiles, isotopic analyses ($\delta^{34}S$, $\delta^{18}O_{SO4}$, δ^2H_{H2O}, $\delta^{18}O_{H2O}$,

26 and tritium), mineralogical determinations, and molecular biology tools (16S

27 rDNA amplification and sequencing). The origin of dissolved SO_4^{2-} in water is

28 related to pyrite oxidation from Lower Cretaceous sediments, and secondary

29 gypsum dissolution. Under the lake, dissolved SO_4^{2-} decreases with depth,

30 controlled by three main processes: (1) seasonal evaporation cycles, (2)

31   hydrodynamic instability caused by the different density-driven groundwater
32   flow, and (3) sulfate-reduction processes, i.e. dissimilatory bacterial sulfate
33   reduction (BSR). These processes control the continuous recycling of sulfur in
34   the system. Lake water and groundwater are in hydraulic connection, and a
35   density-driven flow (DDF) is able to transport reactive organic matter and
36   dissolved SO_4^{2-} towards the underlying aquifer. Hydrochemical evolution in
37   depth, H_2S production (up to 0.024 nmol/cm^3·s) and the presence of sulfate-
38   reducing bacteria suggest the existence of BSR processes. However, isotope
39   techniques are insufficient to elucidate BSR processes since their isotopic effect
40   is masked by low isotope fractionation and high SO_4^{2-} concentrations. The
41   pattern here described may be found in other saline basins worldwide.

42

43   Highlights

44   Dissolved sulfate is derived from pyrite oxidation and secondary gypsum
45   dissolution in Lower Cretaceous sediments.

46   Dissolved sulfate concentrations are controlled by evaporation, mixing, and
47   bacterial sulfate reduction.

48   Mixing is driven by a density-driven flow towards the underlying aquifer.

49   The isotopic effect of bacterial sulfate reduction is masked.

50   Hydrogen sulfide microprofiles and molecular techniques suggested the
51   occurrence of bacterial sulfate reduction processes.

52

53   Keywords

56

57

1. Introduction

59 Sulfur (S) is the fourteenth most abundant element in the Earth's crust, with an

60 average abundance of 260 μg/g (Schlesinger, 2005). Sulfur exists in sediments

61 as organic and inorganic forms such as metal sulfides (e.g. pyrite, marcasite),

62 sulfate-bearing minerals (e.g. gypsum or anhydrite), and dissolved sulfate.

63 There is evidence that sulfur plays a crucial role in biogeochemical processes

64 since it is a significant electron donor and acceptor in many bacterial

65 metabolisms (Jørgensen, 1988; Holmer and Storkholm, 2001; Glombitza et al.,

66 2013). Sulfur transformations carried by microbes are closely linked with the

67 carbon cycle, particularly sulfate (SO_4^{2-}) reduction coupled to organic carbon

68 oxidation in anoxic environments. Dissimilatory Bacterial Sulfate Reduction

69 (BSR) is a significant mineralization pathway. Almost half of sedimentary

70 organic matter in marine sediments is metabolized with sulfate, which is

71 subsequently reduced to sulfide (Jørgensen, 1982). The main product of BSR

72 processes is hydrogen sulfide (H_2S). However, dissolved sulfide also exists as a

73 bisulfide ion (HS^-) and a sulfide ion (S^{2-}), depending on pH conditions. Only

74 10% of H_2S derived from sulfate reduction is buried in sediment as sulfides (e.g.

75 pyrite), with most of the H_2S re-oxidized again to SO_4^{2-}. Jørgensen (1982)

76 estimated that up to half of the oxygen uptake in sediments could be consumed

77 for sulfide re-oxidation. Sulfide may be oxidized to sulfate through several

78 intermediates (sulfite, thiosulfate, elemental sulfur), which can be dismutated to

79 produce sulfate and sulfide by microbial disproportionation (Bak and Cypionka,

80 1987; Canfield and Thamdrup, 1994). Large amounts of sulfate are released

81 either from re-oxidation of sulfides during the desiccation of wetlands or by

82 chemolithotrophic denitrification in nitrate-polluted areas (Lamers et al., 2001;

83 and references therein). Several risks can be linked to sulfide oxidation, such as

84 the release of heavy metals and metalloids to the environment (Corkhill et al.,

85 2008).

86 Sulfur cycling is of major interest in the field of marine, estuarine, and lake

87 ecosystems for various reasons: (1) gypsum dissolution is an important source

88 of sulfate for microorganisms in evaporitic deposits (Machel, 2001); (2) SO_4^{2-}

89　concentrations can exceed 2,600 mg/L in marine waters and can be even

90　higher in continental saline systems (70,000 mg/L, Kulp et al., 2006); and (3)

91　sulfur derives from human activities such as mining (sulfide ores), fossil fuel

92　emissions and agriculture (fertilizers) (Brimblecombe et al., 1989). Since sulfate

93　is a common constituent of agricultural fertilizers (Vitòria et al., 2004; Oren et

94　al., 2004), human practices in agricultural regions have increased the amount of

95　SO_4^{2-} in aquatic systems (Zak et al., 2009; Baldwin and Mitchell, 2012).

96　Over the past century, stable sulfur isotopes have been used to determine the

97　sources and processes affecting the speciation of sulfur compounds (Thode et

98　al., 1949). There is a large variation of $\delta^{34}S$ in nature: for instance, sulfides

99　usually range from -5‰ to +10‰, terrestrial evaporites usually range from -

100　15‰ to +10‰, and marine evaporites have higher values of +10‰ to +35‰

101　(Krouse and Grinenko, 1991; Clark and Fritz, 1997; Nordstrom et al., 2007).

102　Due to that variation, the sulfur isotope composition ($\delta^{34}S$) of dissolved SO_4^{2-}

103　has been used as an environmental tracer in hydrological systems. More

104　recently, coupling the isotope analyses of sulfur and oxygen of dissolved SO_4^{2-}

105　has allowed a better identification and quantification of sulfate sources (Krouse

106　and Mayer, 2000; Tichomirowa et al., 2010; Li et al., 2011). Isotope techniques

107　have also been applied to trace processes in the biogeochemical sulfur cycle.

108　The natural distribution of sulfur isotopes is controlled mainly by the

109　fractionation imparted by dissimilatory BSR (Chambers and Trudinger, 1979;

110　Canfield, 2001). BSR processes cause fractionation in both the S and O

111　isotopes of dissolved SO_4^{2-}, increasing the isotope composition of S and O in

112　the remaining sulfate at known $\varepsilon^{34}S/\varepsilon^{18}O$ ratios between about 0.6 and 4.3

113　(Böttcher et al., 1998; Brunner et al., 2005). Fractionation of sulfur isotopes can

114　be also caused by microbial sulfur disproportionation: depletions down to 37‰

115　for sulfide, and enrichments up to 35‰ for sulfate (Habicht et al., 1998; Böttcher

116　et al., 2005). Sulfur isotope fractionation is also observed during gypsum

117　precipitation with enrichments up to 2.0‰ (Van Driessche et al., 2016).

118　Conversely, sulfide oxidation causes insignificant isotope fractionation for

119　$\delta^{34}S_{SO4}$ (Habicht et al., 1998), as well as other abiotic processes such as the

120　dissolution of sulfate minerals from evaporites (Claypool et al., 1980). These

121 pathways can be observed in the sedimentary sulfur cycle (Jørgensen, 1990;
122 Werne et al., 2004), as well as in the pelagial sulfur cycle in systems dominated
123 by phototrophic bacteria (Overmann et al., 1996). The use of oxygen isotopes
124 not only in dissolved SO_4^{2-}, but also in water, helps to understand the
125 biogeochemical processes affecting sulfate fate (Craig, 1961).

126 This paper aims to provide insights on the sulfur cycle in a hypersaline lake-
127 aquifer system affected by significant anthropogenic activities. Pétrola Lake is
128 one of the most representative saline wetlands in the Castilla-La Mancha
129 Region (High Segura Basin, SE Spain). However, the lake is disturbed by
130 agricultural activities and urban wastewater discharges, which empty directly
131 into the body of water. These practices are among the most frequently stated
132 problems leading to the degradation of inland wetlands since they can alter the
133 natural saline system by modifying the mass balance and the intensity of
134 biogeochemical processes. Therefore, studying the processes controlling sulfur
135 recycling can help to understand the saline lake-aquifer relationship and the
136 biogeochemical processes involved, improving the characterization of water
137 resources. Preliminary results using hydro-chemical and isotopic tools
138 suggested that S cycling in Pétrola basin depended on the relationship between
139 BSR kinetics and the hydrodynamic instability driven by a density-driven flow
140 (DDF) (Valiente et al., 2017). This approach showed limited results in
141 elucidating S recycling in this hypersaline system. Omoregie et al., (2013)
142 showed the usefulness of combining geochemical, stable isotopes and
143 microbiological data in an acid mine drainage-derived lake. A similar approach
144 was adopted in the present paper, including hydro-chemical and isotopic tools
145 on surface and groundwater samples and on sediment samples as well as the
146 addition of molecular biology tools, in order to identify sulfate sources and the
147 processes taking place in the system.

148

149 ## 2. Study Area

150 The hydrogeological boundary of the Pétrola Lake–aquifer system extends over
151 43 km^2 (Fig. 1). The lake itself occupies the terminal discharge zone of an

152 endorheic basin in a semiarid area, with various small streams discharging into
153 the lake in a radial pattern. The region is characterized by irregular rainfall, long
154 episodes of drought, and torrential precipitation. Pétrola Lake is located in the
155 southeastern Castilla-La Mancha region, and is part of the Segura River Basin.
156 Farming (cultivation, raising livestock) is the main economic activity in the area.
157 According to the European database Corine Land Cover 2000 (European
158 Environment Agency, Copenhagen), irrigation and dry land occupy about
159 17 km^2, which represents 40% of the total basin surface. Crops are fertilized
160 mainly using inorganic fertilizers. Urban wastewater (from a population of 850
161 inhabitants) is discharged, untreated, directly to the lake.

162 The lake occupies about 1.76 km^2 and is shallow, its depth nowhere exceeding
163 2 meters (In Spanish: Confederación Hidrográfica del Segura, unpublished
164 data). In 2007, the total volume of groundwater withdrawals from the Pétrola
165 hydrogeological boundary was 2 Mm^3/year. Water volume in the Pétrola Lake
166 shows oscillations mainly depending on the climatic events. Seasonal
167 fluctuations show a maximum water volume at early spring (reaching about 0.90
168 hm^3 in February), concurring with abundant precipitation and low evaporation
169 rates, and a minimum volume (or completely dryness) at the end of summer,
170 related to few precipitation events and maximum evaporation rates (López-
171 Donate et al., 2004). The work of Vicente et al. (1998) has shown that chemical
172 hydrofacies changes slightly between early spring (Mg-Cl-SO$_4$) and early fall
173 (Mg-Na-Cl-SO$_4$). The same chemical composition (Mg-Na-Cl-SO$_4$) was found in
174 summer by Ordóñez et al. (1973).

175 The basin geology comprises mainly Mesozoic materials (Utrilla et al., 1992).
176 The bottom of the sequence is formed of oolitic carbonate Jurassic rocks. The
177 base of the Lower Cretaceous unit corresponds to the Weald Facies and
178 consists of argillaceous sediments overlain by sands and sandy-conglomerate
179 sediments with intergranular porosity, which reaches the Barremian. Albian
180 deposits (Utrillas Facies) consist of siliciclastic sands, sandy-conglomerates,
181 and reddish to dark-grey clay to argillaceous sediments deposited over Aptian
182 sediments. The Utrillas Facies comprises sandy-conglomerate sediments
183 interstratified by grey-to-black argillaceous sediments with organic matter and

184 sulfides (mainly pyrite). The main aquifer is formed of Lower Cretaceous
185 sediments (Utrillas Facies) comprising siliciclastic sands, conglomerates, and
186 siltstones with a thickness that can exceed 60 metres. Groundwater flow in this
187 aquifer is radial and centripetal from the recharge areas (basin margins) to the
188 lake (Gómez-Alday et al., 2014). In a saline lake–aquifer interface, the
189 difference in density between the brine from the lake and fresh groundwater can
190 produce a density-driven flow (DDF) from saline lake water towards the
191 underlying aquifer (Zimmermann et al., 2006). In previous studies using
192 electrical resistivity tomography in Pétrola Lake, Gomez-Alday et al. (2014)
193 observed the existence of a dense brine perched on less dense fresh
194 groundwater as a result of DDF, caused by the instability of the saline boundary
195 layer.

196 ---------------------------------- Fig. 1 near here ---
197 -

198

199 **3. Materials and Methods**

200 **3.1 Sampling**

201 Four PVC piezometers were installed in the lake in September 2008 following a
202 radial pattern from the eastern lake margin (SE, GW-34) towards the lake
203 center (NW, GW-26) (Fig. 2). The depth profiles and screened intervals of each
204 piezometer are detailed in Figure 2. The piezometers are 5 cm in inner
205 diameter, and were installed at different depths: 12.1 m (GW-12), 25.8 m (GW-
206 26), 34.1 m (GW-34), and 37.9 m (GW-38). Screen lengths are 4 m (GW-12), 9
207 m (GW-26), 5 m (GW-34), and 3 m (GW-38). Screening zones were isolated by
208 internal bentonite seals. A total of 37 water samples were collected between
209 September 2008 and October 2011 from five control points: four piezometers
210 and surface water (SW-0). Simultaneous measurements of groundwater level
211 were performed for piezometers GW-12, GW-26, and GW-34 using a ceramic
212 CTD-Diver stand-alone sensor (piezometer GW-38 is an artesian well, so it was
213 not measured). Data were collected from February 2010 to October 2011 at 24-
214 hour intervals (n=609 daily measurements). Precipitation data for the study

215 period were acquired from meteorological station AB07 (Ministry of Agriculture

216 and Fisheries, Food and Environment of Spain) in Pozo Cañada, about 16 km

217 from Pétrola Lake.

218 ----------------------------------- Fig. 2 near here ---

219 Sediment samples (n=13) were taken from the cores recovered during

220 piezometer construction (Fig. 2, samples ANNA-1 to ANNA-22). The sediment

221 cores were collected at eight different depths from 3.4 to 37.3 metres below

222 ground surface (mbgs). All the samples were preserved in frozen polypropylene

223 tubes with dry ice at -80°C, stored in polyethylene bags, closed, and shipped to

224 the laboratory. Simultaneously, another 12 samples from an evaporitic crust

225 were collected following a linear transect from the depocenter (sample PE MIN

226 1, next to a breakwater) to the eastern margin of the lake (sample PE MIN 12)

227 at intervals of 15 meters (Fig. 1C). Furthermore, seven samples of secondary

228 gypsum were collected from several silt deposits belonging to Lower

229 Cretaceous sediments, cropping out in the study area (Fig. 1C). Three cores

230 from the upper 20 cm of recent organic-rich sediments deposited on the lake

231 bottom were collected for DNA extraction and microprofiling using Plexiglass

232 coring tubes (5 cm inner diameter and 20 cm long) in January 2016. Each

233 coring tube was capped at top and bottom with silicone rubber, cooled, and

234 immediately taken to the laboratory following the methodology of Kondo et al.

235 (2004).

236

237 **3.2 Chemical analyses**

238 Physical-chemical parameters were measured in situ with portable electrodes

239 (n=32). The control parameters were water temperature (T), pH, electrical

240 conductivity (EC), redox potential (Eh), and dissolved oxygen (DO). In surface

241 water, measurements were performed directly, whereas in the four piezometers

242 measurements were made using a flow-through chamber to minimize the effect

243 of air exchange. Water samples were stored at 4°C in darkness prior to further

244 analysis following official standard methods (APHA-AWWA-WEF, 1998). Water

245 samples for major ions were filtered with a 0.45 µm nylon Millipore® filter. For

246 the determination of dissolved organic carbon (DOC), Fe and Mn, samples were

247 filtered with a 0.20 µm nylon Millipore® filter. Alkalinity determinations were

248 carried out in the laboratory by acid–base titration. HCO_3^-, SO_4^{2-}, and Cl^-

249 contents were measured by ion chromatography (DX120, Vertex). Na^+, K^+,

250 Ca^{2+}, Mg^{2+}, total Fe, and Mn concentrations were measured in an atomic

251 absorption spectrophotometer equipped with an air-acetylene burner. DOC

252 concentrations were determined using a Shimadzu Analyzer in the research

253 services at the University of A Coruña.

254 ### 3.3 Isotope analyses

255 Isotope analyses were performed for 34 water samples. Isotope ratios of sulfur

256 ($^{34}S/^{32}S$) and oxygen ($^{18}O/^{16}O$) from dissolved SO_4^{2-} were measured on $BaSO_4$

257 precipitated by the addition of 5% $BaCl_2 \cdot 2H_2O$ and HCl, boiling it to prevent

258 $BaCO_3$ precipitation (Dogramaci et al., 2001). The $\delta^{34}S_{SO4}$ was analysed in a

259 Carlo Erba Elemental Analyzer (EA) coupled in continuous flow to a Finnigan

260 Delta C IRMS at the "Centres Científics i Tecnològis" at the Universitat de

261 Barcelona (CCiT-UB). The $\delta^{18}O_{SO4}$ values were analysed in duplicate with a

262 ThermoQuest high-temperature conversion analyzer (TC/EA) unit with a

263 Finnigan MAT Delta C IRMS at the CCiT-UB. $^{18}O/^{16}O$ ratios from H_2O were

264 measured by the CO_2 equilibration method using a Multiflow device coupled in

265 line to a continuous flow Isoprime Mass Spectrometer. The δ^2H_{H2O} values were

266 obtained by measuring H_2 in the reduction of Cr with an elemental analyzer

267 (EuroVector) with a continuous flow mass spectrometer (Isoprime Mass

268 Spectrometer) at the LIE-US. $\delta^{18}O_{H2O}$ and δ^2H_{H2O} determinations were carried

269 out at the Stable Isotopes Laboratory at the University of Salamanca (LIE-US).

270 Radioactive isotopes of H^3 (tritium) in groundwater were determined by liquid

271 scintillation (n=5) counting in ^{14}C and the Tritium Dating Service at the

272 Autonomous University of Barcelona.

273 Furthermore, isotopes were analysed in 37 solid samples. The $\delta^{34}S$ values from

274 gypsum and sulfide were determined on Ag_2S as described by Canfield et al.

275 (1986) and Hall et al. (1988). These analyses were performed in a SIRA-II dual

9

276 inlet spectrometer at the LIE-US. The $\delta^{18}O$ values from gypsum samples were
277 also analysed in duplicate with a ThermoQuest high-temperature conversion
278 analyzer (TC/EA). Results are reported in δ values relative to international
279 standards (Vienna Canyon Diablo Troilite (VCDT) for $\delta^{34}S$ and Vienna Standard
280 Mean Ocean Water (VSMOW) for $\delta^{18}O$ and δ^2H. Analytical reproducibility by
281 repeated analyses of both international and internal reference samples of
282 known isotopic composition is determined to be about ± 0.2‰ for $\delta^{34}S$, ± 0.5‰
283 for $\delta^{18}O$ of SO_4^{2-}, ± 0.3‰ for $\delta^{18}O$ in water, ± 1‰ for δ^2H in water, and ± 0.4 for
284 Tritium Units (TU).

285 *3.4 Mineral identification*

286 Sediment samples from piezometer cores (n=8) and recent evaporitic crusts
287 from the lake bottom (n=12) were analysed using electronic microscopy (ZEISS
288 DSM 940) and X-ray diffraction (Bruker-AXS D5005). For this purpose, thin
289 films were obtained from the solid samples. The microscopy analyses were
290 performed at the Rock Preparation Service of the University of Salamanca. The
291 X-ray diffraction analyses were performed at the Jaume Almera Earth Sciences
292 Institute at the Spanish National Research Council (ICTJA-CSIC). Saturation
293 indices (SI) of minerals were calculated using the PHREEQC thermodynamic
294 software (Parkhurst and Appelo, 1999). The SI was calculated for halite (NaCl),
295 gypsum ($CaSO_4 \cdot 2H_2O$), hexahydrite ($CaSO_4 \cdot 6H_2O$), and epsomite ($CaSO_4 \cdot$
296 $7H_2O$) using the Pitzer database (recommended for saline environments;
297 Wolery et al., 2004).

298 *3.5 Hydrogen sulfide microprofiles*

299 Hydrogen sulfide activity in recent organic matter-rich sediments was evaluated
300 by means of H_2S microprofiles. Microprofiles were measured using an H_2S
301 amperometric microelectrode (Unisense A/S, Denmark) with a tip diameter of
302 100 µm. Measurements were taken on individual fresh sediment cores (n=3)
303 collected during January 2016 as described above. Cores were stabilized using

304 lake water for a period not longer than 24 hours. All profiles were carried out at
305 50 µm intervals to reach a depth of 1 centimeter. Microprofile measurements
306 and H_2S activity calculations were performed using dedicated software
307 (SensorTrace Pro v.2.8.2, Unisense A/S, Denmark). To calculate H_2S
308 consumption and production, the method published by Berg et al. (1998) was
309 used assuming steady-state conditions where transport of solutes occurs by
310 diffusion.

311 **3.6 DNA extraction, 16S rDNA amplification, sequencing and phylogenetic**
312 **analysis**

313 Molecular techniques were used for bacterial identification. Aliquots of 50 g
314 (n=3) of recent organic sediment were collected from the top 2 cm of the cores
315 when microprofiling was finished. Then, aliquots of sediment were
316 homogenized. For enrichment, a sulfate-reducing bacteria culture medium was
317 prepared (Pfennig et al., 1981) and supplemented with 7% NaCl and 1%
318 $MgCl_2 \cdot 6H_2O$ (Caumette et al., 1991). Bacteria enrichments (n=3) were
319 inoculated with 1 g of each aliquot of homogenized sediment and incubated at
320 30ºC for 14 days. DNA extraction from enriched cultures was performed using a
321 Bacterial Genomic DNA Isolation Kit (Canvax). Nucleic acid purity was
322 determined by scanning spectrophotometry (Sambrook et al., 1989).

323 DNA extracts were mixed into a single sample and used to amplify fragments of
324 16S rRNA gene (16S rDNA) by polymerase chain reaction (PCR). In a first step,
325 16S rDNA fragments were amplified via PCR using a set of specific
326 oligonucleotide primers DSV435F and DSV1430R for sulfate-reducing bacteria
327 from the *Desulfovibrionaceae* family, following Tanaka et al. (2002).
328 Amplifications were performed in 30 µL volumes with 1.75–2.50 µg of purified
329 DNA template, 1 X PCR buffer (Canvax), 2.5 mM $MgCl_2$, 0.8 mM concentrations
330 of each deoxynucleoside triphosphate, 0.75 mM concentrations of each primer
331 (IDT), and 1 U of Horse-Power Taq DNA polymerase (Canvax). In addition,
332 10% of polyvinylpyrrolidone was added to the PCR mixture to enhance PCR
333 performance (Koonjul et al., 1999). Reactions were carried out using a GenePro

334 (Bioer) cycler in order to control the following PCR conditions: one cycle at 95ºC

335 for 15 min, denaturation at 94°C for 1 min, annealing at 55°C for 1 min,

336 extension at 72°C for 1 min for 35 cycles, and a final extension step at 72ºC for

337 10 min. The resulting PCR product was sequenced (seq1).

338 A second PCR was performed using DNA extracts and a primer set designed

339 by the authors. The second set of primers (DHF and DHR) was designed based

340 on an alignment of 16S rDNA from various strains belonging to *Desulfovibrio*

341 genus from saline environments. Forward primer DHF (5'-

342 TTATGGGGGAAAGGTGGCCT-3'; *Escherichia coli* positions 158-177) was

343 used in combination with reverse primer DHR (5'-

344 CCTGTTTGCTACCCACGCTT-3'; *E. coli* positions 761-742). The specificity of

345 DHF and DHR primers was tested before use using the BLAST software

346 (Altschul et al., 1997) at GenBank to ensure no matches were found with other

347 bacterial 16S rDNA. PCR contained composition described above. Second PCR

348 was performed as follows: a first step at 90ºC for 5 min, denaturation at 95°C for

349 30 s, annealing at 54°C for 40 s, extension at 72°C for 1 min for 35 cycles, and

350 a final extension step at 72ºC for 10 min. Finally, aliquots (1, 2, and 3 µL) of the

351 second PCR product were analysed on a 1% (w/v) denaturing agarose gel

352 electrophoresis, visualized with 1X RedSafe^{TM} (iNtRON Biotechnology) and

353 compared to a 2 µL sub sample of 1 Kb molecular DNA ladder (Invitrogen,

354 USA). The remaining volume of second PCR product was used for sequencing

355 (seq2). The sampling preparation and analytical procedure was performed at

356 the Institute for Regional Development (University of Castilla-La Mancha).

357 Sequencing was carried out using an Applied Biosystems 3730xl DNA Analyzer

358 with 3730xl DNA Analyzer 96-Capillary Array (50 cm) by Macrogen Inc.

359 Each 16S rDNA sequence was compared using Blast from NCBI (Camacho et

360 al., 2009). The closest 16S rDNA sequences were aligned using Clustal Omega

361 (Sievers et al., 2011). Phylogenetic trees were constructed using the Maximum

362 Likelihood method based on the Tamura-Nei distance with the program MEGA7

363 (Kumar et al., 2016). Robustness of the phylogenetic results was checked by

364 bootstrap (1000 replicates). Sequences have been submitted to GenBank under

365 accession numbers MF682361 and MF682362.

366

4. Results

4.1 Hydrogeology

Groundwater level in the piezometers is affected by precipitation events and regional groundwater potential. In GW-12, the level is generally influenced by variations in the lake, mainly related to local precipitation patterns (Fig. 3). The levels also reflect variations in the regional groundwater flow (RGF) potential for February 2010 to October 2011. In piezometer GW-12, groundwater levels noticeably decreased from end of June 2010 to mid-November 2010, coinciding with the end of the dry months. Then, levels dramatically increased from November 2010 to June 2011, coinciding with a period of regular precipitation. Levels fell again during the last months of 2011. The evolution of water levels in GW-26 shows an increasing trend from the end of June 2010 to mid-November 2010. In contrast to shallow piezometers, the groundwater evolution in GW-34 largely reflects variations in the regional groundwater potential.

------------------------------------ Fig. 3 near here --

Tritium levels (Table 1) in water samples range from 0.2 ±0.4 TU to 4.6 ±0.3 TU (n=5), with the highest values in surface lake water (SW-0), reaching 4.6 ±0.3 TU. The shallowest piezometer (GW-12) shows the highest tritium levels in groundwater (1.5 ±0.3 TU), whereas GW-34 yields the lowest (0.2 ±0.4 TU).

------------------------------------ Table 1 near here --

4.2 Hydrochemistry

Table 2 shows the mean values of the chemical analyses for each control point. The detailed results of the chemical analyses for each sample (n=36) are presented as Supplementary Information (Appendix A). Average pH values range from 7.0 (in piezometer GW-34) to 8.1 (in surface water samples, SW-0). The average EC ranges from 2,743 µS/cm (in the deepest piezometer, GW-38),

13

393   to 83,300 µS/cm (SW-0). Average Eh values are between +3 mV (in the

394   shallowest piezometer, GW-12) and +148 mV (SW-0). The average DO ranges

395   from 0.2 mg/L (in piezometer GW-34) to 3.6 mg/L (SW-0). The average DOC

396   concentration ranges from 3.2 mg/L (in the deepest piezometer, GW-38) to

397   305 mg/L (SW-0).

398   ----------------------------------- Table 2 near here --------------------------------------

399   All major ions except Ca^{2+} show minimum average concentrations in the

400   deepest piezometer (GW-38), with maximum concentrations found in surface

401   water (SW-0). Surface water also shows the highest standard deviations in all

402   the major ions. The average SO_4^{2-} concentration ranges from 1,140 mg/L to

403   69,300 mg/L, whereas average Cl^- is between 240 mg/L and 50,800 mg/L. The

404   HCO_3^- contents show a minimum average value of 411 mg/L and a maximum

405   average value of 1,074 mg/L. The average Na^+ contents range from 122 mg/L

406   to 34,800 mg/L, whereas K^+ contents range from 12.9 mg/L to 5,130 mg/L. Mg^{2+}

407   ranges between 165 mg/L and 38,500 mg/L, both in SW-0 samples. Ca^{2+} shows

408   a different depth pattern from Mg^{2+}, with minimum average values of 183 mg/L

409   in the deepest piezometer (GW-38), but maximum values (637 mg/L) at depth

410   (GW-26) instead of at the surface. Mn concentrations do not follow the same

411   trend as the major ions; samples are below the detection limit in surface water

412   and the highest average contents (Mn up to 11.8 µg/L and Fe up to 263 µg/L)

413   are in the deepest piezometer (GW-38). These data were used to determine

414   sample water types. As shown in Figure 4, water type varies between Mg-Ca-

415   SO_4-HCO_3 water (GW-38) and Mg-Na-SO_4-Cl water (SW-0).

416   ------------------------------------ Fig. 4 near here --

4.3 Isotope data

417

418   The isotope analyses of water samples are presented in Table 3. $\delta^{34}S_{SO4}$ in the

419   water samples ranges from −25.9‰ (in the deepest piezometer, GW-38) to

420   −16.2‰ (in piezometer GW-34), with an average value of −21.7‰ (n=15). The

421   average $\delta^{34}S_{SO4}$ shows little variation with depth, with only the deepest

422   piezometer having significantly lower values. $\delta^{18}O_{SO4}$ in water samples ranges

423 between +6.2‰ and +17.5‰, with an average of +12.5‰ (n=15). A decrease in

424 $\delta^{18}O_{SO4}$ is observed with depth. $\delta^{18}O_{H2O}$ in water samples ranges from −8.8‰ to

425 +4.2‰, with an average of −4.5‰ (n=33), and δ^2H_{H2O} ranges from -52.4‰ to

426 +15.1‰, with an average of −35.2‰ (n=29). Both $\delta^{18}O_{H2O}$ and δ^2H_{H2O} show the

427 same pattern with depth as $\delta^{18}O_{SO4}$, with decreasing values from SW-0 to GW-

428 38. These values are shown in Figure 5, which also includes the Global

429 Meteoric Water Line (GMWL; Craig, 1961) and the weighted average

430 precipitation from Madrid. Madrid was selected as the reference station

431 because most of the precipitation at Pétrola Lake is influenced by European

432 Atlantic fronts. The weighted average precipitation was calculated with data

433 from the International Atomic Energy Agency (IAEA) for the period of 1970 to

434 2006, using the values corresponding to dates with precipitation of over 20 mm

435 (n=79) (Schotterer et al., 1996).

436 ---------------------------------- Table 3 near here ---

437 ---------------------------------- Fig. 5 near here ---

438 Isotope data from sulfate-bearing minerals and sulfides are shown in Table 4.

439 The $\delta^{34}S_{gypsum}$ ranges from −30.3‰ (at 27 mbgs) to -9.9‰ (at 3.4 mbgs), with a

440 mean of −21.2‰ (n=20). The $\delta^{18}O_{gypsum}$ varies from -2.8‰, in secondary

441 gypsum samples, collected from Lower Cretaceous sediments, to +18.2‰ in

442 sulfate-bearing minerals from the evaporitic crust, with a mean of +10.6‰

443 (n=25). The $\delta^{34}S_{sulfide}$ values from piezometers range from −40.5‰ (at 37.3

444 mbgs) to −11.7‰ (at 11 mbgs), with a mean of −30.4‰ (n=12).

445 ---------------------------------- Table 4 near here ---

15

4.4 Mineral identification

Mineral identification analyses corresponding to recent evaporitic crusts from the lake bottom show sulfate minerals of calcium (gypsum, $CaSO_4 \cdot 2H_2O$) and/or magnesium (hexahydrite, $MgSO_4 \cdot 6H_2O$) in all samples. Moreover, epsomite ($MgSO_4 \cdot 7H_2O$) is present in four of the twelve samples; halite occurs in all samples, and quartz is observed in most of the surface sediment samples. No sulfides are found in these sediments.

Core sediments from the piezometers are characterized by high organic matter contents. All the organic sediments are rich in sulfides, mostly pyrite, but sphalerite can also appear, at around 11 mbgs (ANNA-8 and ANNA-12b). Most of the cores have sulfate-bearing minerals such as gypsum, hexahydrite, and starkeyite ($MgSO_4 \cdot 4H_2O$), as well as iron oxides (except sample ANNA-8, at 11 mbgs, where sulfur is only present as a sulfide).

Mean SI values for each sample point are shown in Table 5, which evidences that only gypsum precipitates. The SI_{Gypsum} values calculated from water samples range between -1.03 and 0.67 (both in SW-0). $SI_{Epsomite}$ values range between -3.08 (GW-38) and -0.10 (SW-0). SI_{Halite} values vary between -6.62 (GW-38) and -0.01 (SW-0), and $SI_{Hexahydrite}$ values range between -3.42 (GW-38) and -0.29 (SW-0).

------------------------------------- Table 5 near here ---

4.5 Hydrogen sulfide rates

Complete H_2S microprofiles and detailed zones of production and consumption in the water-sediment interface are shown in Supplementary Information (Appendix B). Concentration of H_2S reaches values up to 3.8 mmol/L at 8 mm depth (Profile 3). Production of H_2S is observed from the first 3 mm, 5 mm and 1 mm for profiles 1, 2 and 3, respectively. Maximum H_2S production reaches values up to 0.024 nmol/cm^3·s (Profile 2), similar to maximum production measured in the rest of sediment cores (0.022 nmol/cm^3·s). Nevertheless, H_2S production is not observed through the whole profile in the studied sediment

16

475   cores. Consumption of H_2S is noticed at narrow zones interspersed with sulfide
476   production areas.

477   ***4.6 16S rDNA amplification and phylogenetic affiliation***

478   The products of the PCR performed with the second primer set (DHF and DHR)
479   were analysed by denaturing agarose gel electrophoresis. Patterns are shown
480   in the Supplementary Information (Appendix C, Figure C1). 16S rDNA
481   amplification using the designed primers for *Desulfovibrio* sp. resulted in
482   products of predicted size (604 bp). Phylogenetic trees are included in
483   Supplementary Information (Appendix C). The determined sequences seq1 and
484   seq2 are closely related to *Desulfovibrio senezii* (accession no. NR_024887.1),
485   a gram-negative bacterium isolated from a solar saltern in California (Tsu et al.,
486   1998). The results reveal that sulfate-reducing bacteria from the
487   *Desulfovibrionaceae* family are present in hypersaline sediments from Pétrola
488   Lake.

489

490   ***5. Discussion***

491   ***5.1. Hydrochemical changes across the salt water-fresh water interface***

492   The variability in surface water and groundwater chemistry can be influenced by
493   climate, anthropogenic factors, biogeochemical (water-rock interaction)
494   processes, as well as fluctuations in water level. Commonly, during wet periods,
495   precipitation can dilute surface water, whereas in dry periods, surface water
496   salinity can increase by evaporation. Seasonality causes chemical variations,
497   which are observed in surface water (SW-0) samples. Those samples from
498   hydrological year 2010 show minimum concentrations of SO_4^{2-} (43,227 mg/L),
499   Cl^- (21,768 mg/L) and DOC (140 mg/L) during high water-level season
500   (February 2010). Maximum concentrations in SW-0 are found during low water-
501   level stage (October 2010): SO_4^{2-} (122,957 mg/L), Cl^- (102,814 mg/L) and DOC
502   (646 mg/L). Regarding groundwater samples, SO_4^{2-}, Cl^- and DOC

503   concentrations decrease from GW-12 to GW-38, but seasonal variations are not

504   observed.

505   Seasonality is also reflected in the $\delta^{18}O_{H2O}$ and δ^2H_{H2O}. Kinetic fractionation

506   processes affect oxygen and hydrogen isotopes differently during evaporation.

507   In arid regions with low relative humidity, the evaporation rate is faster and the

508   deuterium excess of the meteoric water line is higher (Clark and Fritz, 1997).

509   The $\delta^{18}O_{H2O}$ and δ^2H_{H2O} results in the study area show a slope (5.2) consistent

510   with evaporation processes (Fig. 5). Samples from Pétrola basin intercept the

511   GMWL close to the local weighted average precipitation value. Water samples

512   close to the local weighted precipitation value belong to regional fresh

513   groundwater samples (GW-38). Samples from SW-0, GW-12 and GW-26 show

514   a positive shift from the GMWL (Fig. 5). These results indicate that the $\delta^{18}O_{H2O}$

515   and δ^2H_{H2O} observed in surface water are due to the evaporation of rainwater

516   with a similar isotopic composition as the local weighted average precipitation.

517   Groundwater isotopes ($\delta^{18}O_{H2O}$ and δ^2H_{H2O}) from GW-12 and GW-26 show a

518   mixture between evaporated lake saltwater and regional freshwater (GW-38).

519   Hydrochemical evolution across the saltwater-freshwater interface has been

520   studied. Cl^- evolution has been employed as conservative tracer (Fig. 6). The

521   Cl^- concentrations were higher in GW-12 than in surface water for samples

522   taken in February 2010, April 2010, and October 2011. These samples were

523   collected during wet periods due to precipitation events that increase freshwater

524   input into the lake and thereby dilute surface waters. Other processes

525   influencing the trend in Cl^- concentration is the precipitation of Cl-bearing

526   minerals, supported by the identification of halite in lake sediments. On the

527   other hand, samples taken in July, October, and November 2010 show higher

528   EC and Cl^- contents in surface water than in groundwater (GW-12). These

529   results are in agreement with the absence of significant precipitation events in

530   the summer of 2010, in which evaporation processes determined high salt

531   concentrations in the surface water. The intense evaporation processes were

532   also evidenced in July 2010 by means of $\delta^{18}O_{H2O}$ and δ^2H_{H2O}. Then, despite

533   precipitation in autumn 2010 (Fig. 3), Cl^- concentrations measured in October

534   and November 2010 increased up to 103,000 mg/L (Fig. 6). This increase is

535   most likely related to the dissolution of the surficial salts previously precipitated

536   in the lake during previous dry seasons.

537   ------------------------------------ Fig. 6 near here ---

538   The decrease in Cl^- with depth can be explained by a mixing process between

539   lake saltwater (due to DDF) and regional freshwater (RGF represented by GW-

540   38). These Cl^- variations measured in piezometers are also consistent with the

541   isotope composition of $\delta^{18}O_{H2O}$ and δ^2H_{H2O}, where the highest Cl^-

542   concentrations match up with the heaviest isotope values. Despite the

543   significant variations in surface water salinity, and the observed differences in

544   water density (SW-0 has values up to 1.29 g/cm^3, and GW-38 has values

545   around 1.01 g/cm^3), groundwater chemistry remains almost constant suggesting

546   quasi-equilibrium between DDF and RGF during the studied period. The

547   buoyancy of the RGF upwards limits the impact of DDF in solute transport.

548   Sulfate and DOC concentrations are also represented in depth (Fig. 6). The

549   trend of SO_4^{2-} concentrations is similar to that observed for Cl^-. In surface water,

550   SO_4^{2-} concentration can be affected by evaporation, external inputs (streams),

551   precipitation and dissolution of S-bearing minerals, as well as sulfate-reduction

552   processes. In groundwater, the decrease in SO_4^{2-} concentration with depth

553   could be the result of a mixing process between lake saltwater and freshwater

554   from RGF (GW-38), as inferred for Cl^-. However, decrease in SO_4^{2-} is slightly

555   higher than Cl^- decrease in depth in samples from July 2010, October 2010 and

556   November 2010. A possible explanation may be a combined effect of mixing

557   and other processes that decrease the amount of dissolved SO_4^{2-}, such as

558   mineral precipitation or BSR processes. Sulfate reduction can occur in

559   environments with low oxygen and nitrate concentrations, low Eh, and the

560   presence of reactive organic matter (Hem, 1985; Miao et al., 2012). Concerning

561   to organic matter, the highest DOC levels are found in surface water samples.

562   Moreover, the sediment from the bottom of the lake has shown itself to be an

563   important source of organic C (Carrey et al., 2014). DOC concentrations

564   dramatically decrease from surface water to GW-12, mainly related to organic

565   carbon consumption and the availability of organic substrate. DOC contents in

566   GW-12 are still significant and can be derived from the organic matter not

567   consumed in the sediment-water interface from the lake. In the deepest
568   piezometers (GW-34 and GW-38), DOC seems to be related to the organic
569   matter present in the Lower Cretaceous sediments from the Utrillas Facies
570   (Carrey et al., 2013).

571   *5.2 Source of sulfate*

572   Potential sources of sulfate in Pétrola Lake are mainly related with sulfides and
573   sulfates (Fig. 7). In general, $\delta^{34}S$ in all S-bearing species (dissolved SO_4^{2-},
574   sulfide and sulfate-bearing minerals) show negative values (-40‰ to -9.9‰).
575   This range, and the absence of relevant sedimentary evaporite formations in the
576   study area, imply that the main source of sulfur in Pétrola basin is disseminated
577   pyrite in the organic-rich sediments interbedded in the Utrillas Facies (Gómez-
578   Alday et al., 2014). Disseminated secondary gypsum derives from disseminated
579   pyrite oxidation showing $\delta^{34}S$ values (-22.1‰ to -15.7‰) consistent with those
580   observed in the sulfate-bearing minerals from the lake evaporitic crusts (-
581   20.5‰ to -18.3‰).

582   ------------------------------------ Fig. 7 near here ---

583   Sulfide oxidation should theoretically impart negligible isotope fractionation for
584    $\delta^{34}S_{SO4}$ (Habicht et al., 1998), and $\delta^{18}O_{SO4}$ should be derived from oxygen in
585   water and/or air. The sulfide oxidation box in Figure 7 was drawn using
586   maximum and minimum values of $\delta^{34}S_{Sulfide}$, whereas $\delta^{18}O_{SO4}$ was calculated
587   following the equations defined by Van Stempvoort and Krouse (1994) for the
588   theoretical value of dissolved SO_4^{2-} derived from sulfide oxidation. The authors
589   defined a lower value in which all the oxygen in dissolved SO_4^{2-} is derived from
590   water oxygen ($\delta^{18}O_{SO4} = \delta^{18}O_{H2O}$), and an upper limit where part of the sulfate
591   oxygen is derived from water and part from air, and where fractionation in the
592   incorporation of oxygen and water has been considered ($\delta^{18}O_{SO4} =$
593    $0.62 \cdot \delta^{18}O_{H2O} + 9$, Eq. 1). The $\delta^{18}O_{H2O}$ used in Eq. 1 is the average value
594   measured at the corresponding depth throughout the sampling period (2008-
595   2011). The lowest $\delta^{34}S_{Sulfide}$ value (-40.5‰) is found in the deepest sample at
596   37.3 mbgs. Most of the sulfide samples range from -40‰ to -33‰, except three

597 samples collected between 8 mbgs and 11 mbgs (samples ANNA-11b, ANNA-
598 12b and ANNA-22c) that show higher $\delta^{34}S_{Sulfide}$ values, from -19‰ to -11‰.

599 Sulfate-bearing minerals (gypsum) present as secondary mineral in lower
600 Cretaceous sediments and in evaporitic crust (gypsum, hexahydrite, and
601 epsomite) deposited seasonally in the lake are another potential source of
602 dissolved sulfate in the system. Isotopically, samples corresponding to sulfate-
603 bearing minerals show significant variability in $\delta^{34}S_{SO4}$ and $\delta^{18}O_{SO4}$ values.
604 Samples collected from the lake evaporitic crust show a low variance in $\delta^{34}S_{SO4}$
605 (mean value of -20.1‰ ± 0.8‰), whereas $\delta^{18}O_{SO4}$ ranges from +14.3‰ to
606 +18.2‰. The high values of $\delta^{18}O_{SO4}$ in the lake evaporites compared to sulfates
607 derived from sulfide oxidation can be explained by sulfate recycling. Dissolved
608 SO_4^{2-} can undergo sulfate reduction processes, generating H_2S, which can be
609 re-oxidized. Then, dissolved SO_4^{2-} may precipitate during evaporation producing
610 enrichments up to +2.0‰ and +3.6‰ for $\delta^{34}S_{SO4}$ and $\delta^{18}O_{SO4}$, respectively
611 (Lloyd, 1968; Van Driessche et al., 2016). $\delta^{18}O$ values found in the sulfate-
612 bearing minerals deposited in lake evaporites are higher than the expected due
613 to precipitation. These higher values of $\delta^{18}O_{SO4}$ may be explained by variations
614 in the degree of evaporation of surface water and the incorporation of $\delta^{18}O_{H2O}$
615 signal of evaporated water in SO_4^{2-} during H_2S re-oxidization. This is supported
616 by the $\delta^{18}O_{SO4}$ values of the evaporites sampled in the linear transect (PE MIN-
617 1 to PE MIN-12) of the lake, which show slightly lower oxygen values in
618 samples from the lake margin, indicating less evaporated water (PE MIN-10, PE
619 MIN-11) and slightly higher values in evaporites collected closer to the
620 depocenter (PE MIN-1, PE MIN-2), indicating more evaporated water.

621 The isotope composition of sulfate-bearing minerals sampled in the piezometer
622 cores shows more variability. Samples of sulfate-bearing minerals ANNA-17,
623 ANNA-18, and ANNA-20, collected from 27 mbgs to 34 mbgs, show $\delta^{34}S_{SO4}$
624 values between -30‰ and to -20‰, similar to the sulfides sampled at the same
625 depth (Fig. 7). Furthermore, their $\delta^{18}O_{SO4}$ values are in agreement with the
626 precipitation of sulfate derived from sulfide oxidation. Samples ANNA-1 (10.8
627 mbgs) and ANNA-21 (8.4 mbgs) show similar $\delta^{34}S_{SO4}$ values, but their higher
628 $\delta^{18}O_{SO4}$ values cannot be explained from sulfide oxidation in equilibrium with the

629 groundwater. These samples of secondary gypsum were collected at

630 intermediate depths and $\delta^{18}O_{SO4}$ should be interpreted as a mixture between

631 sulfate derived from sulfide oxidation and from sulfate from the dissolved

632 evaporitic crust minerals from the lake, which have a higher $\delta^{18}O_{SO4}$ values.

633 Finally, sample ANNA-22, obtained at 3.4 mbgs, has a $\delta^{34}S_{SO4}$ of -9.9‰ and a

634 $\delta^{18}O_{SO4}$ of +16‰. Since gypsum dissolution has little or negligible isotope

635 fractionation for sulfur and oxygen isotopes (Claypool et al., 1980), the values

636 for sample ANNA-22 cannot be explained by precipitation or dissolution

637 processes. An alternative explanation could be pyrite oxidation with an isotope

638 composition similar to those found at 10 mbgs ($\delta^{34}S_{Sulfide}$ of -11‰, Fig. 7) and a

639 highly water evaporated oxygen signature ($\delta^{18}O_{SO4}$ of +16.4‰).

640 Secondary gypsum sampled from Lower Cretaceous outcrops (PE ARMO

641 samples) show $\delta^{18}O_{SO4}$ values much lower than sulfate-bearing minerals from

642 the evaporitic crust from the lake, but similar to mineral samples collected from

643 deep points in the piezometers (ANNA-17, ANNA-18, and ANNA-20). These

644 $\delta^{18}O_{SO4}$ values from PE ARMO samples (between -2.8‰ and +9.0‰) are close

645 to those calculated for sulfate derived from sulfide oxidation in equilibrium with

646 groundwater according to equation 1 (Van Stempvoort and Krouse, 1994).

647 Moreover, samples PE ARMO-4a and PE ARMO-5 show the highest $\delta^{34}S_{SO4}$

648 and $\delta^{18}O_{SO4}$ of the group. These samples fall close to groundwater samples

649 collected in GW-38, in the area of sulfate derived from sulfide oxidation (Fig. 7).

650 Surface water (SW-0) and groundwater samples GW-12 and GW-26 show

651 $\delta^{34}S_{SO4}$ and $\delta^{18}O_{SO4}$ values inside the area defined by the lake evaporites

652 analysed. No significant differences are observed in the isotope composition of

653 dissolved SO_4^{2-} between sampling dates, suggesting seasonal stability on both

654 sulfate sources and recycling processes.

655 *5.3 Sulfate recycling*

656 For a better understanding of the processes involved in sulfate fate, the isotope

657 composition of S and O from dissolved SO_4^{2-} was compared to sulfate-bearing

658 minerals, and sulfides at different depths (Fig. 8). Additionally, values of $\delta^{18}O_{SO4}$

659 which would be derived from sulfide oxidation following Eq. 1 are also

660   compared. For this purpose, the average $\delta^{18}O_{H2O}$ values of water for each

661   sampling depth are used for the calculation. Surface water samples (SW-0),

662   show the same $\delta^{34}S_{SO4}$ and $\delta^{18}O_{SO4}$ as the sulfate-bearing minerals from the

663   lake's evaporitic crust, and similar $\delta^{34}S_{SO4}$ values to secondary gypsum from

664   Lower Cretaceous sediments (Fig. 8). Despite the changes in depth of the

665   dissolved SO_4^{2-} concentration, no noticeable variation is observed in the isotope

666   composition at SW-0, GW-12, GW-26 and GW-34 (although isotope data is

667   limited). The high SO_4^{2-} concentration buffers the isotope composition and may

668   mask sulfate-reduction processes. In the lake surface, precipitation and

669   dissolution of S-bearing minerals must be also considered. During dry periods,

670   evaporite mineral precipitation occurs, but also the high SO_4^{2-} concentration

671   would mask the slight isotope fractionation of gypsum precipitation. Sulfur

672   evolution in the lake is dominated by the seasonal cycles of mineral

673   precipitation and dissolution, which are common in hypersaline lakes

674   (Cartwright et al., 2009). Then, in wet periods, evaporites are redissolved,

675   increasing SO_4^{2-} concentrations with no significant changes in the isotope

676   values because dissolution produces insignificant isotope fractionation for both

677     $\delta^{34}S_{SO4}$ and $\delta^{18}O_{SO4}$.

678   ------------------------------------- Fig. 8 near here ---

679   In GW-12, both the SO_4^{2-} concentrations as well as the S and O isotope

680   composition of dissolved SO_4^{2-} become stable. The $\delta^{34}S_{SO4}$ is similar to the

681   isotope composition of the sulfate-bearing minerals from piezometer cores,

682   which are also within the range of sulfide minerals collected at this depth (Fig.

683   8). However, $\delta^{18}O_{SO4}$ is clearly higher than the value of sulfate-bearing minerals

684   from the piezometer cores and the theoretical value of sulfate calculated for

685   sulfides at this depth. Sulfate reduction processes cannot explain this high

686     $\delta^{18}O_{SO4}$ values since the $\delta^{34}S_{SO4}$ did not show to be affected by this reaction. S-

687   recycling incorporating higher $\delta^{18}O_{H2O}$ from evaporated water during mixing

688   processes between lake water and fresh water, as suggested by hydrochemical

689   and tritium data (Table 1) could explain this high $\delta^{18}O_{SO4}$ values. The huge

690   SO_4^{2-} concentration at this depth (12.1 mbgs) supports this idea. Thus, the more

691   likely hypothesis is that its origin is related to lake water recharge by DDF. The

692   $\delta^{34}S_{SO4}$ and $\delta^{18}O_{SO4}$ in GW-12 is similar to dissolved SO_4^{2-} in the lake (Fig. 8),

693   supporting this hypothesis. Currently, the system seems to have reached a

694   hydrodynamic equilibrium between surface water, with the associated DDF, and

695   the hydraulic potential of RGF. This assumption is also in agreement with water

696   isotopic data ($\delta^{18}O_{H2O}$ and $\delta^{2}H_{H2O}$) measured in the piezometers (Table 3).

697   Groundwater samples obtained from GW-26 and GW-34 show $\delta^{34}S_{SO4}$ and

698   $\delta^{18}O_{SO4}$ values indicating a mixing trend between GW-12 and GW-38. These

699   results further support the idea of a mixing process between DDF and RGF. In

700   the deepest well (GW-38), $\delta^{34}S_{SO4}$ and $\delta^{18}O_{SO4}$ values are slightly higher than

701   the expected values from sulfide oxidation and close to the ones from

702   secondary gypsum from Lower Cretaceous outcrops. The dissolved SO_4^{2-} found

703   in GW-38 could be derived mainly from secondary gypsum dissolution, which is

704   mixed with the recharge water from the lake. This mixing process is in

705   agreement with the water isotopic values of the samples. Hence, it could

706   conceivably be hypothesized that sulfate derived from sulfide oxidation and

707   secondary gypsum dissolution constantly accumulates in the lake. Seasonal

708   variations affect precipitation and dissolution of S-bearing minerals in lake

709   surface. Dissolved SO_4^{2-} can be also transported to the underlying aquifer by

710   means of DDF.

711   *5.4 Sulfate reduction processes*

712   Evidence of BSR processes is provided by the microprofiling data, which show

713   that H_2S is produced in the first cm of recent organic-rich sediments. Calculated

714   rates of H_2S production (mean of 0.023 nmol/cm^3·s) are similar to those

715   described previously in Pétrola Lake (up to 0.025 nmol/cm^3·s; Menchen et al.,

716   2016), and are also in the range of other lake sediments (about 0.017

717   nmol/cm^3·s; Smith and Klug, 1981), and slightly below saltmarsh sediments (up

718   to 0.033 nmol/cm^3·s; Roychoudhury et al., 2003) and estuarine sediments (up

719   to 0.047 nmol/cm^3·s in closed state system, Richards and Pallud, 2016).

720   Microprofiles of H_2S show well-defined zones for sulfate reduction processes.

721   The limiting factor for these processes are neither the organic matter nor the

722   dissolved SO_4^{2-}. Thus, the shape of the H_2S production curve suggests the re-

723 oxidation of H_2S to SO_4^{2-} in the suboxic zone below the water-sediment

724 interface. Furthermore, as BSR processes take place in the water-sediment

725 interface, a significant part of the produced H_2S is feasible to be re-oxidized

726 again to dissolved SO_4^-. Besides the processes cited above, the formation of

727 sulfur intermediates and further microbial disproportionation must be

728 considered. Microbes responsible for BSR, such as *Desulfobulbus spp.* and

729 *Desulfovibrio spp*, are able to perform disproportionation reactions (Widdel and

730 Pfennig, 1982; Krekeler et al., 1997). Disproportionation of sulfur intermediates

731 would lead to larger isotope fractionations in dissolved SO_4^- with $\delta^{34}S_{SO4}$

732 enrichment up to +35‰ (Böttcher et al., 2005). Moreover, a depletion in $\delta^{34}S$

733 from H_2S should be expected (up to -37‰; Habicht et al., 1998). Nevertheless,

734 measurements of H_2S and sulfur intermediates were not performed. Thus, data

735 is insufficient to make any assumption about the presence of microbial

736 disproportionation in recent organic-rich sediments from Pétrola Lake.

737 Assuming the existence of sulfate-reducing processes, values of $\delta^{34}S$ and

738 $\delta^{18}O_{SO4}$ from water samples (SW-0, GW-12, and GW-26) and mineral samples

739 (lake evaporites) can be explained. In dissimilatory BSR, DOC acts as an

740 electron donor, reducing sulfate under anaerobic conditions (Nordstrom et al.,

741 2007), and the rate of sulfate reduction is typically C-limited (Madigan, 1997).

742 Anaerobic conditions and high DOC concentrations are found in surface and

743 piezometer water samples (Appendix A). Dissolved oxygen values show anoxic

744 conditions, with minimum values of 0.26 mg/L in surface water, 0.03 mg/L in the

745 shallowest piezometer (GW-12), and 0.08 mg/L in the one immediately below

746 (GW-26). The main sources of DOC in lake water, with values up to 646 mg/L in

747 surface water (October 2010), are the degradation of autochthonous (primary

748 productivity of the lake) and allochthonous (wastewater) sources (Gómez-Alday

749 et al., 2014). Organic matter deposition has shown a high capacity to promote

750 reducing conditions in batch and column experiments (Carrey et al., 2014). In

751 fact, the amount of organic C present in the sediment can be as high as 23%

752 (Valiente et al., 2016). Previous laboratory experiments have also shown the

753 high capacity of organic-rich sediments to promote reducing conditions (Carrey

754 et al., 2013). In the sampled surface water and groundwater, NO_3^-

755 concentrations are negligible and oxygen is limited, so the main electron
756 acceptor is dissolved SO_4^{2-}. These conditions are favourable for sulfate
757 reduction (Champ et al., 1979).

758 Isotopically, BSR results in an increase in both the $\delta^{34}S_{SO4}$ and $\delta^{18}O_{SO4}$.
759 Assuming that this reaction follows a Rayleigh distillation in a closed system, a
760 negative relationship between $Ln[SO_4^{2-}]$ and $\delta^{34}S_{SO4}$ and $\delta^{18}O_{SO4}$ would be
761 expected (Spence et al., 2001). However, the samples show the opposite trend:
762 an increase in $\delta^{34}S_{SO4}$ and $\delta^{18}O_{SO4}$ as $Ln[SO_4^{2-}]$ increases. One feasible
763 hypothesis to explain the lack of correlation, even when chemical data indicate
764 favourable conditions for sulfate reduction, is that the large amount of SO_4^{2-} in
765 surface and groundwater could mask the isotope shift associated to BSR.
766 Furthermore, traces of sulfide and a faint odour of H_2S were occasionally noted
767 during surface water sampling, suggesting sulfate reduction, that was confirmed
768 by microprofiling.

769 Biologically, 16S rDNA amplification was successful using two set of 16S rDNA-
770 targeted primers of sulfate-reducing bacteria. Sequencing confirms the
771 presence of sulfate-reducing bacteria belonging to *Desulfovibrionaceae* family
772 (seq-1) and to *Desulfovibrio* genus (seq-2). However, the results do not discard
773 the presence of other bacterial communities able to reduce sulfate in lake
774 sediments. These results complement the hypothesis of BSR processes in the
775 hypersaline sediments of Pétrola Lake. Prior studies that have noted the low
776 isotope fractionation for $\delta^{34}S$ (ε=-2.0‰) produced by bacteria from genus
777 *Desulfovibrio* in hypersaline mats (*D. halophilus*; Detmers et al., 2001).
778 Therefore, the low variability in the isotope composition observed in the
779 samples can also be attributed to the low isotope fractionation.

780 Based on the surface water and groundwater samples (SW-0, GW-12, and GW-
781 26) with the highest $\delta^{34}S_{SO4}$ and $\delta^{18}O_{SO4}$ values, a simplified model has been
782 calculated for the evolution of SO_4^{2-} concentrations and $\delta^{34}S$ isotope
783 composition during BSR (Fig. 9).No data was found in the literature about
784 isotope fractionation for $\delta^{34}S$ produced by the closest microorganism reported
785 by phylogenetic analyses (*D. senezii*). Thus, the reported isotope fractionation
786 for *D. halophilus* was used for calculation: a 40% complete sulfate reduction is

787   needed to produce a 1‰ shift in $\delta^{34}S_{SO4}$. Consequently, taking into account the

788   high SO_4^{2-} concentration of the samples, the isotope effect of BSR is masked.

789   The evolution of $\delta^{18}O_{SO4}$ does not agree with a BSR model, and a negative

790   correlation between $\delta^{18}O_{SO4}$ and $1/[SO_4^{2-}]$ is observed (R^2=0.94), suggesting

791   that mixing rather than other processes is controlling $\delta^{18}O_{SO4}$. This may be

792   influenced by the constant cycles of evaporation and dissolution in surface

793   water that also mask the relationship between isotope composition and SO_4^{2-}

794   concentration.

795   ----------------------------------- Fig. 9 near here --

796

797   **6. Conclusions**

798   In the Pétrola Lake-aquifer system, the continuous recycling of sulfur is

799   controlled by three main processes: (1) seasonal evaporation cycles, (2)

800   hydrodynamic instability driven by the different density-driven groundwater flow,

801   and (3) sulfate-reduction processes (BSR). Sulfate distribution is controlled by

802   evaporation (due to seasonal drought) and mixing processes (from a DDF

803   towards the underlying aquifer). Hydrochemical and isotopic evolution in depth

804   indicate that lake water and groundwater are in hydraulic connection, and DDF

805   is able to transport reactive organic matter and other solutes (e.g. SO_4^{2-}) from

806   the lake to the underlying aquifer. Despite seasonal variations found in surface

807   water, SO_4^{2-} concentrations and $\delta^{34}S_{SO4}$ become almost constant during the

808   study period in the piezometers, suggesting quasi-equilibrium between DDF

809   and RGF. Sulfate in Pétrola Lake is originally derived from: (1) oxidation of

810   disseminated pyrite present in the Lower Cretaceous sediments, and (2)

811   dissolution of secondary gypsum derived from sulfide oxidation in Lower

812   Cretaceous sediments. The presence of sulfate-reducing bacteria belonging to

813   *Desulfovibrionaceae* family and the detected production of H_2S in the first cm of

814   sediment, confirm the occurrence of BSR processes. Nevertheless, the isotope

815   effect of BSR is masked due to low isotope fractionation and the large amount

816   of dissolved SO_4^{2-} in surface water and groundwater. The analysis of sulfur

817   dynamics undertaken here has extended our knowledge of the sulfur cycle in a

818   hypersaline system. Further work could focus on the interaction between S-

27

819 cycle and pollutants attenuation (e.g. nitrate), as well as other potential biotic

820 processes (e.g. microbial disproportionation) in Pétrola hypersaline lake-aquifer

821 system.

822

823
824 ***Acknowledgments***

836

837 ***References***

838 Alpers, C. N., Rye, R. O., Nordstrom, D. K., White, L. D., King, B. S., 1992.

839 Chemical, crystallographic and stable isotopic properties of alunite and jarosite

840 from acid—Hypersaline Australian lakes. Chem. Geol. 96 (1-2), 203-226.

841 http://dx.doi.org/10.1016/0009-2541(92)90129-S

842 Altschul, S. F., Madden, T. L., Schäffer, A. A., Zhang, J., Zhang, Z., Miller, W.,

843 Lipman, D. J., 1997. Gapped BLAST and PSI-BLAST: a new generation of

844 protein database search programs. Nucleic Acids Res. 25 (17), 3389-3402.

845 http://dx.doi.org/10.1093/nar/25.17.3389

846 APHA-AWWA-WEF, 1998. Standard methods for the examination of water and

847 wastewater. American Public Health Association, Washington, DC (1998), p.

848 1268.

849   Bak, F., Cypionka, H., 1987. A novel type of energy metabolism involving
850   fermentation of inorganic sulphur compounds. Nature 326 (6116), 891-892.
851   http://dx.doi.org/10.1038/326891a0

852   Baldwin, D. S., Mitchell, A., 2012. Impact of sulfate pollution on anaerobic
853   biogeochemical cycles in a wetland sediment. Water Res. 46 (4), 965-974.
854   http://dx.doi.org/10.1016/j.watres.2011.11.065

855   Berg, P., Risgaard-Petersen, N., Rysgaard, S., 1998. Interpretation of
856   measured concentration profiles in sediment pore water. Limnol. Oceanogr. 43
857   (7), 1500-1510. http://dx.doi.org/10.4319/lo.1998.43.7.1500

858   Böttcher, M. E., Usdowski, E., 1993. $^{34}S/^{32}S$ ratios of the dissolved sulphate of
859   river, well and spring waters in a gypsum-carbonate karst area at the southwest
860   edge of the Harz mountains. Z. Dtsch. Geol. Ges. 144, 471–477.

861   Böttcher, M. E., Brumsack, H. J., De Lange, G. J., 1998. Sulfate reduction and
862   related stable isotope (^{34}S, ^{18}O) variations in interstitial waters from the Eastern
863   Mediterranean. In: Proceedings of the Ocean Drilling Program (ODP), Sci. Res.
864   A. H. F. Robertson, K. C. Emeis & A. Camerlenghi (eds.). Vol 160: 365-376.

865   Böttcher, M. E., Thamdrup, B., Gehre, M., Theune, A., 2005. 34S/32S and
866   18O/16O fractionation during sulfur disproportionation by Desulfobulbus
867   propionicus. Geomicrobiol.   J. 22   (5),   219-226.
868   http://dx.doi.org/10.1080/01490450590947751

869   Brimblecombe, P., Hammer, C., Rodhe, H., Ryaboshapko, A., Boutron, C. F.,
870   1989. Human influence on the sulphur cycle. In: Evolution of the global
871   biogeochemical sulphur cycle, 77-121.

872   Brunner, B., Bernasconi, S. M., Kleikemper, J., Schroth, M. H., 2005. A model
873   for oxygen and sulfur isotope fractionation in sulfate during bacterial sulfate
874   reduction processes. Geochim. Cosmochim. Ac. 69 (20), 4773-4785.
875   http://dx.doi.org/10.1016/j.gca.2005.04.017

876   Camacho, C., Coulouris, G., Avagyan, V., Ma, N., Papadopoulos, J., Bealer, K.,
877   Madden, T. L., 2009. BLAST+: architecture and applications. BMC
878   Bioinformatics 10(1), 421. http://dx.doi.org/10.1186/1471-2105-10-421

879   Canfield, D. E., Raiswell, R., Westrich, J. T., Reavesy, C. M., Berner, R. A.,

880   1986. The use of chromium reduction in the analysis of reduced inorganic sulfur

881   in sediments and shales. Chem. Geol. 54 (1), 149-155.

882   http://dx.doi.org/10.1016/0009-2541(86)90078-1

883   Canfield, D. E., Thamdrup, B., 1994. The production of (34) S-depleted sulfide

884   during bacterial disproportionation of elemental sulfur. Science 266 (5193),

885   1973. http://dx.doi.org/10.1126/science.11540246

886   Canfield, D. E., 2001. Isotope fractionation by natural populations of sulfate-

887   reducing bacteria. Geochim. Cosmochim. Acta, 65(7), 1117-1124.

888   http://dx.doi.org/10.1016/S0016-7037(00)00584-6

889   Carrey, R., Otero, N., Soler, A., Gómez-Alday, J. J., Ayora, C., 2013. The role of

890   Lower Cretaceous sediments in groundwater nitrate attenuation in central

891   Spain: Column experiments. Appl. Geochem. 32, 142-152.

892   http://dx.doi.org/10.1016/j.apgeochem.2012.10.009

893   Carrey, R., Rodríguez-Escales, P., Otero, N., Ayora, C., Soler, A., Gómez-

894   Alday, J. J., 2014. Nitrate attenuation potential of hypersaline lake sediments in

895   central Spain: Flow-through and batch experiments. J. Contam. Hydrol. 164,

896   323-337. http://dx.doi.org/10.1016/j.jconhyd.2014.06.017

897   Cartwright, I., Hall, S., Tweed, S., Leblanc, M., 2009. Geochemical and isotopic

898   constraints on the interaction between saline lakes and groundwater in

899   southeast Australia. Hydrogeol. J. 17 (8), 1991-2004.

900   http://dx.doi.org/10.1007/s10040-009-0492-5

901   Caumette, P., Cohen, Y., Matheron, R., 1991. Isolation and characterization of

902   Desulfovibrio halophilus sp. nov., a halophilic sulfate-reducing bacterium

903   isolated from Solar Lake (Sinai). Syst. Appl. Microbiol. 14 (1), 33-38.

904   http://dx.doi.org/10.1016/S0723-2020(11)80358-9

905   Chambers, L. A., Trudinger, P. A., 1979. Microbiological fractionation of stable

906   sulfur isotopes: a review and critique. Geomicrobiol. J. 1 (3), 249-293.

907   http://dx.doi.org/10.1080/01490457909377735

908   Champ, D. R., Gulens, J., Jackson, R. E., 1979. Oxidation–reduction
909   sequences in ground water flow systems. Can. J. Earth Sci. 16 (1), 12-23.
910   http://dx.doi.org/10.1139/e79-002

911   Clark, I. D., Fritz, P., 1997. Environmental isotopes in hydrogeology. CRC
912   press.

913   Claypool, G. E., Holser, W. T., Kaplan, I. R., Sakai, H., Zak, I., 1980. The age
914   curves of sulfur and oxygen isotopes in marine sulfate and their mutual
915   interpretation. Chem.   Geol. 28,   199-260.   http://dx.doi.org/10.1016/0009-
916   2541(80)90047-9

917   Corkhill, C. L., Wincott, P. L., Lloyd, J. R., Vaughan, D. J., 2008. The oxidative
918   dissolution of arsenopyrite (FeAsS) and enargite (Cu 3 AsS 4) by Leptospirillum
919   ferrooxidans.   Geochim.   Cosmochim.   Ac.   72   (23),   5616-5633.
920   http://dx.doi.org/10.1016/j.gca.2008.09.008

921   Craig, H., 1961. Isotopic variations in meteoric waters. Science 133 (3465),
922   1702-1703. http://dx.doi.org/10.1126/science.133.3465.1702

923   Detmers, J., Brüchert, V., Habicht, K. S., Kuever, J., 2001. Diversity of sulfur
924   isotope fractionations by sulfate-reducing prokaryotes. Appl. Environ. Microb.
925   67(2): 888-894. http://dx.doi.org/10.1128/AEM.67.2.888-894.2001

926   Dogramaci, S. S., Herczeg, A., Schiffy, S., Bone, Y., 2001. Controls on δ^{34}S
927   and δ^{18}O of dissolved sulfate in aquifers of the Murray Basin, Australia and their
928   use as indicators of flow processes. Appl. Geochem. 16 (4), 475-488.
929   http://dx.doi.org/10.1016/S0883-2927(00)00052-4

930   Glombitza, C., Stockhecke, M., Schubert, C. J., Vetter, A., Kallmeyer, J., 2013.
931   Sulfate reduction controlled by organic matter availability in deep sediment
932   cores from the saline, alkaline Lake Van (Eastern Anatolia, Turkey). Front.
933   Microbiol. 4, 209. http://dx.doi.org/10.3389/fmicb.2013.00209

934   Gómez-Alday, J. J., Carrey, R., Valiente, N., Otero, N., Soler, A., Ayora, C.,
935   Sanz, D., Muñoz-Martín, A., Castaño, S., Recio, C., Carnicero, A., Cortijo, A.,
936   2014. Denitrification in a hypersaline lake–aquifer system (Pétrola Basin,
937   Central Spain): The role of recent organic matter and Cretaceous organic rich

938 sediments. Sci. Total Environ. 497, 594-606.
939 http://dx.doi.org/10.1016/j.scitotenv.2014.07.129

940 Habicht, K. S., Canfield, D. E., Rethmeier, J., 1998. Sulfur isotope fractionation
941 during bacterial reduction and disproportionation of thiosulfate and sulfite.
942 Geochim. Cosmochim. Ac. 62 (15), 2585-2595.
943 http://dx.doi.org/10.1016/S0016-7037(98)00167-7

944 Hall, G. E., Pelchat, J. C., Loop, J., 1988. Separation and recovery of various
945 sulphur species in sedimentary rocks for stable sulphur isotopic determination.
946 Chem. Geol. 67 (1), 35-45. http://dx.doi.org/10.1016/0009-2541(88)90004-6

947 Hem, J. D., 1985. Study and interpretation of the chemical characteristics of
948 natural water (Vol. 2254). Department of the Interior, US Geological Survey.

949 Holmer, M., Storkholm, P., 2001. Sulphate reduction and sulphur cycling in lake
950 sediments: a review. Freshwater Biol. 46 (4), 431-451.
951 http://dx.doi.org/10.1046/j.1365-2427.2001.00687.x

952 Jørgensen, B. B., 1982. Mineralization of organic matter in the sea bed-the role
953 of sulphate reduction. Nature 296, 643-645. http://dx.doi.org/10.1038/296643a0

954 Jørgensen, B. B., 1988. Ecology of the sulphur cycle: oxidative pathways in
955 sediments. The nitrogen and sulphur Cycles, 42, 31-63.

956 Jørgensen, B. B., 1990. The sulfur cycle of freshwater sediments: role of
957 thiosulfate. Limnol. Oceanogr. 35 (6), 1329-1342.
958 http://dx.doi.org/10.4319/lo.1990.35.6.1329

959 Kondo, R., Nedwell, D. B., Purdy, K. J., Silva, S. Q., 2004. Detection and
960 enumeration of sulphate-reducing bacteria in estuarine sediments by
961 competitive PCR. Geomicrobiol. J. 21 (3), 145-157.
962 http://dx.doi.org/10.1080/01490450490275307

963 Koonjul, P. K., Brandt, W. F., Lindsey, G. G., Farrant, J. M., 1999. Inclusion of
964 polyvinylpyrrolidone in the polymerase chain reaction reverses the inhibitory
965 effects of polyphenolic contamination of RNA. Nucleic Acids Res. 27 (3), 915-
966 916. http://dx.doi.org/10.1093/nar/27.3.915

967 Krekeler, D., Sigalevich, P., Teske, A., Cypionka, H., Cohen, Y., 1997. A
968 sulfate-reducing bacterium from the oxic layer of a microbial mat from Solar
969 Lake (Sinai), Desulfovibrio oxyclinae sp. nov. Arch. Microbiol. 167 (6), 369-375.
970 http://dx.doi.org/10.1007/s002030050

971 Kroopnick, P., Craig, H., 1972. Atmospheric oxygen: isotopic composition and
972 solubility   fractionation. Science 175   (4017),   54-55.
973 http://dx.doi.org/10.1126/science.175.4017.54

974 Krouse, H. R., Grinenko, V. A., 1991. Stable isotopes: natural and
975 anthropogenic sulphur in the environment, SCOPE 48. John Wiley and Sons
976 Ltd, New York, USA

977 Krouse, H. R., Mayer, B., 2000. Sulphur and oxygen isotopes in sulphate. In:
978 Environmental   tracers   in   subsurface   hydrology,   Springer: 195-231.
979 http://dx.doi.org/10.1007/978-1-4615-4557-6_7

980 Kulp, T. R., Hoeft, S. E., Miller, L. G., Saltikov, C., Murphy, J. N., Han, S.,
981 Oremland, R. S., 2006. Dissimilatory arsenate and sulfate reduction in
982 sediments of two hypersaline, arsenic-rich soda lakes: Mono and Searles
983 Lakes,   California. Appl.   Environ.   Microb. 72   (10),   6514-6526.
984 http://dx.doi.org/10.1128/AEM.01066-06

985 Kumar, S., Stecher, G., Tamura, K., 2016. MEGA7: Molecular Evolutionary
986 Genetics Analysis version 7.0 for bigger datasets. Mol. Biol. Evol. 33 (7), 1870-
987 1874. http://dx.doi.org/10.1093/molbev/msw054

988 Lamers, L. P., Ten Dolle, G. E., Van Den Berg, S. T., Van Delft, S. P., Roelofs,
989 J. G., 2001. Differential responses of freshwater wetland soils to sulphate
990 pollution.   Biogeochemistry   55   (1),   87-101.
991 http://dx.doi.org/10.1023/A:1010629319168

992 Li, X. D., Liu, C. Q., Liu, X. L., Bao, L. R., 2011. Identification of dissolved
993 sulfate sources and the role of sulfuric acid in carbonate weathering using dual-
994 isotopic data from the Jialing River, Southwest China. J. Asian Earth Sci. 42 (3),
995 370-380. http://dx.doi.org/10.1016/j.jseaes.2011.06.002

996   Lloyd, R. M., 1968. Oxygen isotope behavior in the sulfate-water system. J.
997   Geophys. Res. 73 (18), 6099-6110. http://dx.doi.org/10.1029/JB073i018p06099

998   López-Donate, J. A., Montesinos-Ibáñez, J. G., López-Cano, J. A., Martínez-
999   Núñez, J. C., 2004. Estudio descriptivo del sector endorreico-salino de Pétrola,
1000   Corral Rubio y La Higuera (Albacete). In: II Jornadas sobre el Medio Natural
1001   Albacetense, 357-370.

1002   Machel, H. G., 2001. Bacterial and thermochemical sulfate reduction in
1003   diagenetic settings—old and new insights. Sediment. Geol. 140 (1), 143-175.
1004   http://dx.doi.org/10.1016/S0037-0738(00)00176-7

1005   Madigan, M. T., Martinko, J. M., Parker, J., 1997. Brock biology of microbiology.
1006   Prentice Hall, New Jersey, USA.

1007   Menchen, A., Valiente, N., Gomez-Alday, J. J., 2016. O2 and H2S
1008   microrespiration processes in the sediment-water interface from Pétrola
1009   hypersaline lake (SE Albacete). 33rd SIL Congress, Turin.

1010   Miao, Z., Brusseau, M. L., Carroll, K. C., Carreón-Diazconti, C., Johnson, B.,
1011   2012. Sulfate reduction in groundwater: characterization and applications for
1012   remediation. Environ. Geochem. Hlth. 34 (4), 539-550.
1013   http://dx.doi.org/10.1007/s10653-011-9423-1

1014   Nordstrom, D. K., Wright, W. G., Mast, M. A., Bove, D. J., Rye, R. O., 2007.
1015   Aqueous-sulfate stable isotopes—a study of mining-affected and undisturbed
1016   acidic drainage. US Geological Survey Professional Paper 1651: 387-416.

1017   Omoregie, E., Santofimia, E., López-Pamo, E., Wegener, G., Böttcher, M.,
1018   Escher, P., Struck, U., Aguilera, A., Amils, R., 2013. Biogeochemistry of Acidic
1019   Lakes in the Iberian Pyritic Belt. Mineral. Mag. 77 (5), 1890.

1020   Ordóñez, S., García del Cura, M. A., Marfil, R., 1973. Sedimentación actual: la
1021   laguna de Pétrola (Albacete). Est. Geol. 29, 367-377.

1022   Oren, O., Yechieli, Y., Böhlke, J. K., Dody, A., 2004. Contamination of
1023   groundwater under cultivated fields in an arid environment, central Arava Valley,
1024   Israel. J. Hydrol. 290 (3), 312-328.
1025   http://dx.doi.org/10.1016/j.jhydrol.2003.12.016

1026 Overmann, J., Beatty, J. T., Krause, H. R., Hall, K. J., 1996. The sulfur cycle in
1027 the chemocline of a meromictic salt lake. Limnol. Oceanogr. 41 (1), 147-156.
1028 http://dx.doi.org/10.4319/lo.1996.41.1.0147

1029 Parkhurst, D.L., Appelo, C., 1999. User's guide to PHREEQC (Version 2): A
1030 computer program for speciation, batch-reaction, one-dimensional transport,
1031 and inverse geochemical calculations. USGS water-resources investigations
1032 report: 99-4259.

1033 Pfennig, N., Widdel, F., Trüper, H. G., 1981. The dissimilatory sulfate-reducing
1034 bacteria. In The prokaryotes (pp. 926-940). Springer Berlin Heidelberg.
1035 http://dx.doi.org/10.1007/978-3-662-13187-9_74

1036 Richards, C. M., Pallud, C., 2016. Kinetics of sulfate reduction and sulfide
1037 precipitation rates in sediments of a bar-built estuary (Pescadero,
1038 California). Water   Res. 94,   86-102.
1039 http://dx.doi.org/10.1016/j.watres.2016.01.044

1040 Roychoudhury, A. N., Van Cappellen, P., Kostka, J. E., Viollier, E., 2003.
1041 Kinetics of microbially mediated reactions: dissimilatory sulfate reduction in
1042 saltmarsh sediments (Sapelo Island, Georgia, USA). Estuar. Coast. Shelf S. 56
1043 (5), 1001-1010. http://dx.doi.org/10.1016/S0272-7714(02)00325-6

1044 Sambrook, J., Fritsch, E. F., Maniatis, T., 1989. Molecular cloning: a laboratory
1045 manual, 2nd edn. Cold Spring Laboratory Press. New York.

1046 Schlesinger, W. H., 2005. Biogeochemistry (Vol. 8). Gulf Professional
1047 Publishing.

1048 Schotterer, U., Oldfield, F., Fröhlich, K., 1996. GNIP. Global Network for
1049 Isotopes in Precipitation.

1050 Sievers, F., Wilm, A., Dineen, D., Gibson, T. J., Karplus, K., Li, W., Lopez, R.,
1051 McWilliam, H., Remmert, M., Söding, J., Thompson, J. D., Higgings, D. G.,
1052 2011. Fast, scalable generation of high-quality protein multiple sequence
1053 alignments using Clustal Omega. Mol. Syst. Biol. 7 (1), 539.
1054 http://dx.doi.org/10.1038/msb.2011.75

1055   Smith, R. L., Klug, M. J., 1981. Reduction of sulfur compounds in the sediments
1056   of a eutrophic lake basin. Appl. Environ. Microb. 41 (5), 1230-1237.

1057   Spence, M. J., Bottrell, S. H., Thornton, S. F., Lerner, D. N., 2001. Isotopic
1058   modelling of the significance of bacterial sulphate reduction for phenol
1059   attenuation in a contaminated aquifer. J. Contam. Hydrol. 53 (3), 285-304.
1060   http://dx.doi.org/10.1016/S0169-7722(01)00170-X

1061   Tanaka, Y., Sogabe, M., Okumura, K., Kurane, R., 2002. A highly selective
1062   direct method of detecting sulphate-reducing bacteria in crude oil. Lett. Appl.
1063   Microbiol. 35 (3), 242-246. http://dx.doi.org/10.1046/j.1472-765X.2002.01175.x

1064   Thode, H. G., Macnamara, J., Collins, C. B., 1949. Natural variations in the
1065   isotopic content of sulphur and their significance. Can. J. Res. 27 (4), 361-373.
1066   http://dx.doi.org/10.1139/cjr49b-038

1067   Tichomirowa, M., Heidel, C., Junghans, M., Haubrich, F., Matschullat, J., 2010.
1068   Sulfate and strontium water source identification by O, S and Sr isotopes and
1069   their temporal changes (1997–2008) in the region of Freiberg, central-eastern
1070   Germany. Chem. Geol. 276 (1), 104-118.
1071   http://dx.doi.org/10.1016/j.chemgeo.2010.06.004

1072   Tsu, I. H., Huang, C. Y., Garcia, J. L., Patel, B. K., Cayol, J. L., Baresi, L., Mah,
1073   R. A., 1998. Isolation and characterization of Desulfovibrio senezii sp. nov., a
1074   halotolerant sulfate reducer from a solar saltern and phylogenetic confirmation
1075   of Desulfovibrio fructosovorans as a new species. Arch. Microbiol. 170 (4), 313-
1076   317. http://dx.doi.org/10.1007/s002030050

1077   Utrilla, R., Pierre, C., Orti, F., Pueyo, J. J., 1992. Oxygen and sulphur isotope
1078   compositions as indicators of the origin of Mesozoic and Cenozoic evaporites
1079   from Spain. Chem. Geol. 102 (1), 229-244. http://dx.doi.org/10.1016/0009-
1080   2541(92)90158-2

1081   Valiente, N, Menchen, A., Jirsa, F., Hein, T., Wanek, W., Gómez-Alday, J. J.,
1082   2016. Biogeochemical processes of nitrate in Pétrola Basin: a saline lake-
1083   aquifer system. 33rd SIL Congress, Turin.

1084 Valiente, N., Menchen, A., Carrey, R., Otero, N., Soler, A., Sanz, D., Gomez-
1085 Alday, J. J., 2017. Sulfur recycling processes in a eutrophic hypersaline system:
1086 Pétrola Lake (SE, Spain). Proced. Earth Plan. Sc. 17, 201-204.
1087 http://dx.doi.org/10.1016/j.proeps.2016.12.071

1088 Van Driessche, A. E. S., Canals, A., Ossorio, M., Reyes, R. C., García-Ruiz, J.
1089 M., 2016. Unraveling the Sulfate Sources of (Giant) Gypsum Crystals Using
1090 Gypsum Isotope Fractionation Factors. J. Geol. 124 (2), 235-245.
1091 http://dx.doi.org/10.1086/684832

1092 Van Stempvoort, D., Krouse, H., 1994. Controls of ^{18}O in Sulfate: Review of
1093 Experimental Data and Application to Specific Environments. ACS Symposium
1094 Series, American Chemical Society.

1095 Vicente, E., Miracle, M. R., 1998. Estudio limnológico de 28 humedales de
1096 Castilla-La Mancha como base para la elaboración del Plan de Ordenación de
1097 Recursos Naturales (P.O.R.N.). Unpublished technical report.

1098 Vitòria, L., Otero, N., Soler, A., Canals, À., 2004. Fertilizer characterization:
1099 isotopic data (N, S, O, C, and Sr). Environ. Sci. Technol. 38 (12), 3254-3262.
1100 http://dx.doi.org/10.1021/es0348187

1101 Werne, J. P., Hollander, D. J., Lyons, T. W., Damsté, J. S. S., 2004. Organic
1102 sulfur biogeochemistry: recent advances and future research directions. Geol.
1103 S. Am. S. 379, 135-150. http://dx.doi.org/10.1130/0-8137-2379-5.135

1104 Widdel, F., Pfennig, N., 1982. Studies on dissimilatory sulfate-reducing bacteria
1105 that decompose fatty acids II. Incomplete oxidation of propionate by
1106 Desulfobulbus propionicus gen. nov., sp. nov. Arch. Microbiol. 131 (4), 360-365.
1107 http://dx.doi.org/10.1007/BF00411187

1108 Wolery, T., Jove-Colon, C., Rard, J., Wijesinghe, A., 2004. Pitzer database
1109 development: Description of the Pitzer geochemical thermodynamic database
1110 data0. ypf. Appendix I in In-Drift Precipitates/Salts Model (P. Mariner) Report
1111 ANL-EBS-MD-000045 REV, 2.

1112 Zak, D., Rossoll, T., Exner, H. J., Wagner, C., Gelbrecht, J., 2009. Mitigation of
1113 sulfate pollution by rewetting of fens—A conflict with restoring their phosphorus
1114 sink function? Wetlands 29 (4), 1093-1103. http://dx.doi.org/10.1672/09-102D.1

1115 Zimmermann, S., Bauer, P., Held, R., Kinzelbach, W., Walther, J.H., 2006. Salt
1116 transport on islands in the Okavango Delta: Numerical investigations. Adv.
1117 Water Resour. 29 11–29. http://dx.doi.org/10.1016/j.advwatres.2005.04.013

Tracing sulfate recycling in the hypersaline Pétrola Lake (SE Spain): A combined isotopic and microbiological approach

N. Valiente[a], R. Carrey[b], N. Otero[b,c], M.A. Gutiérrez-Villanueva[a], A. Soler[b], D. Sanz[a], S. Castaño[a], and J.J. Gómez-Alday[a]

a Biotechnology and Natural Resources Section, Institute for Regional Development (IDR), University of Castilla–La Mancha (UCLM), Campus Universitario s/n, 02071 Albacete, Spain

b Grup d'Mineralogia Aplicada i Medi Ambient, Dep. Mineralogia, Petrologia i Geologia Aplicada, Facultat de Ciències de la Terra, Universitat de Barcelona (UB), C/ Martí i Franquès s/n, 08028, Barcelona, Spain

c Serra Hunter Fellowship, Generalitat de Catalunya, Spain

Figure captions

Figure	Caption
Figure 1.	A) Location of Castilla-La Mancha region. B) Pétrola endorheic basin and Pétrola Lake. C) Geological map of Pétrola Basin and location of sample points: 1. SW-0; 2. Transect of PE MIN solid samples; 3. Piezometers; 4. PE ARMO 2; 5. PE ARMO 3; 6. PE ARMO 4 a and PE ARMO 4 b; 7. PE ARMO 5; 8. PE ARMO 6; 9. PE ARMO 7.
Figure 2.	Map with the location of SW-0 and piezometers in Pétrola Lake. Piezometers follow a radial pattern from the lake margin (SE, GW-34, x: 624943.5, y: 4299678.2) towards the lake center (NW, GW-26, x: 624921.9, y: 4299674.6), separated at 6 meters' equidistance. The simplified hydrogeological cross-section I–I′ shows the geology below the lake and the location of the piezometers. Mineral samples (ANNA-1 to ANNA-22) from the cores are indicated in the piezometers map. AB: anoxic brine. masl: meters above sea level. mbgs: meters below ground surface.
Figure 3.	Groundwater depth profiles in GW-12, GW-26, and GW-34 piezometer (lines). Precipitation (P) between February-2010 and October-2011 (bars). Electrical conductivity (EC) profiles in the piezometers in mS/cm are shown for the studied period.
Figure 4.	Piper diagram showing the chemical composition of the water samples during the studied period.
Figure 5.	Regression line for $\delta^{18}O_{H2O}$ and δ^2H_{H2O} values in water samples (n=29) collected from piezometers and surface water. GMWL: Global Meteoric Water Line (Craig, 1961). WP: weighted precipitation from Madrid.

Figure 6.	Hydrochemical profiles: sulfate (SO_4^{2-}), chloride (Cl^-), and dissolved organic carbon (DOC), from samples collected in the piezometers and surface water: a) February 2010; b) April 2010; c) July 2010; d) October 2010; e) November 2010; f) October 2011.
Figure 7.	$\delta^{34}S_{SO4}$ versus $\delta^{18}O_{SO4}$ plot. The evaporite lake area is defined by the maximum and minimum analysed values for $\delta^{34}S$ and $\delta^{18}O$ in sulfate-bearing mineral samples from the lake. The sulfate oxidation area is defined by the maximum and minimum analysed values for $\delta^{34}S$, as well as the maximum and minimum calculated values for $\delta^{18}O$ derived from sulfide oxidation (Van Stempvoort and Krouse, 1994). The fertilizer area is adapted from Vitòria et al. (2004). Atmospheric $\delta^{18}O$ value is defined in the literature (Kroopnick and Craig, 1972). Sulfate-bearing minerals from: e.c.: evaporite crust; p.c.: piezometer cores; s.c.: secondary gypsum.
Figure 8.	A) $\delta^{34}S$ vs depth of dissolved sulfate, sulfides, and sulfate-bearing minerals from lake, piezometers, and basin outcrops. B) $\delta^{18}O$ vs depth of dissolved sulfate, sulfate-bearing minerals from lake, piezometers, and basin outcrops, and $\delta^{18}O$ values calculated following the upper limit equations (Eq. 1) of Van Stempvoort and Krouse (1994) using the higher $\delta^{18}O_{H2O}$ measured at the corresponding depth throughout the sampling period.
Figure 9.	$\delta^{34}S_{SO4}$ vs SO_4^{2-} concentration for SW-0, GW-12, and GW-26 sampling points. The graph shows simplified models of the evolution of sulfate concentration and $\delta^{34}S$ values during BSR using isotope fractionation of -2‰.

Figure2
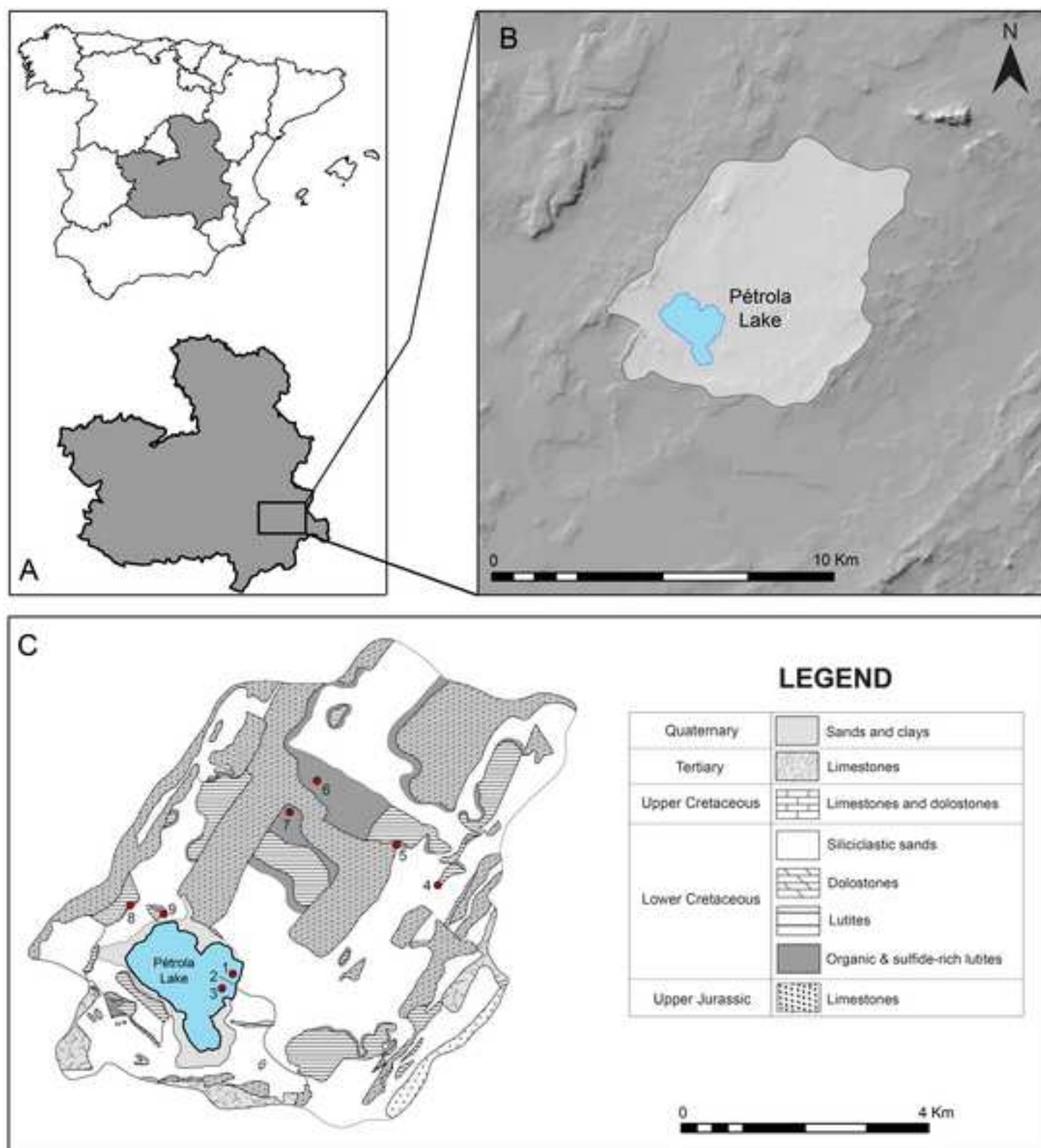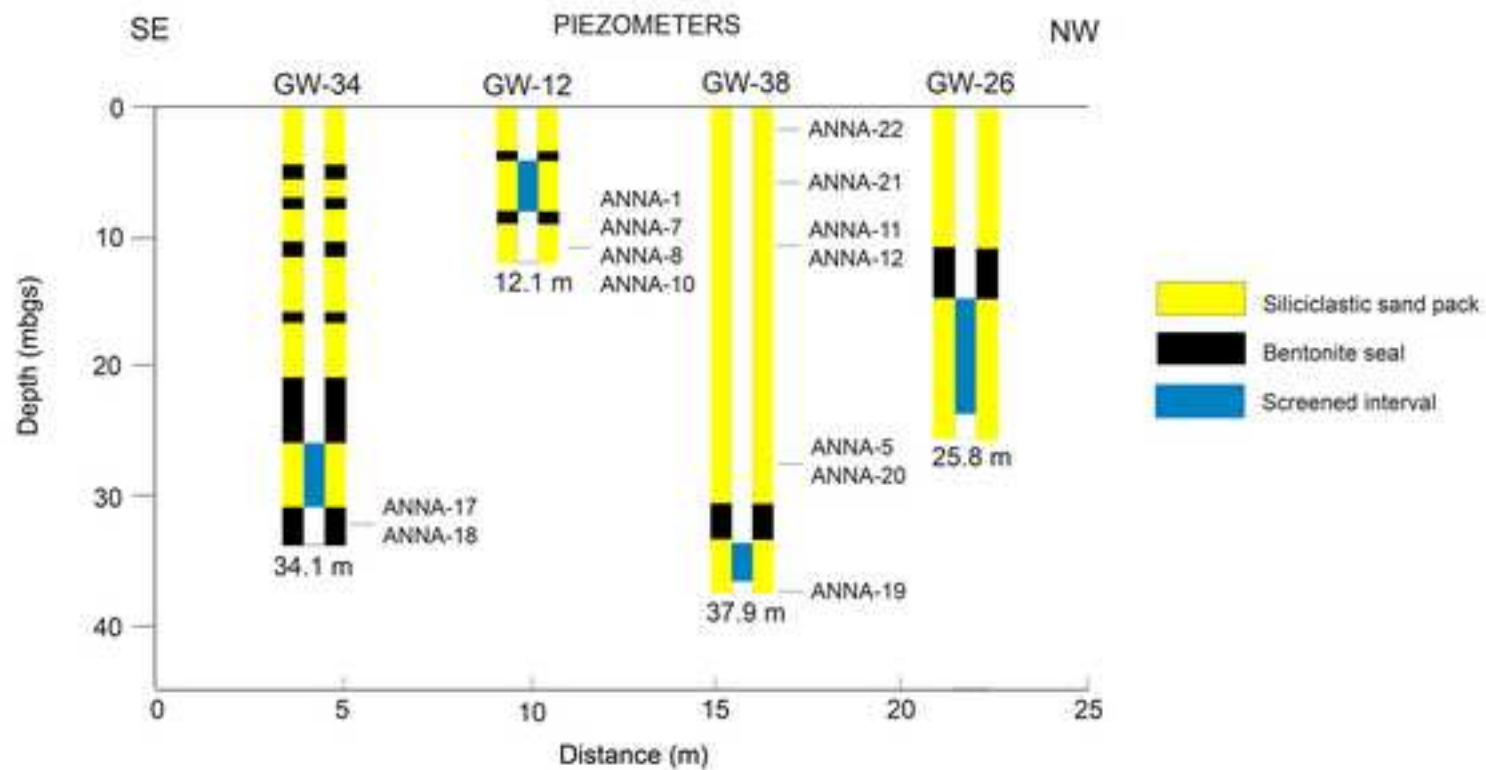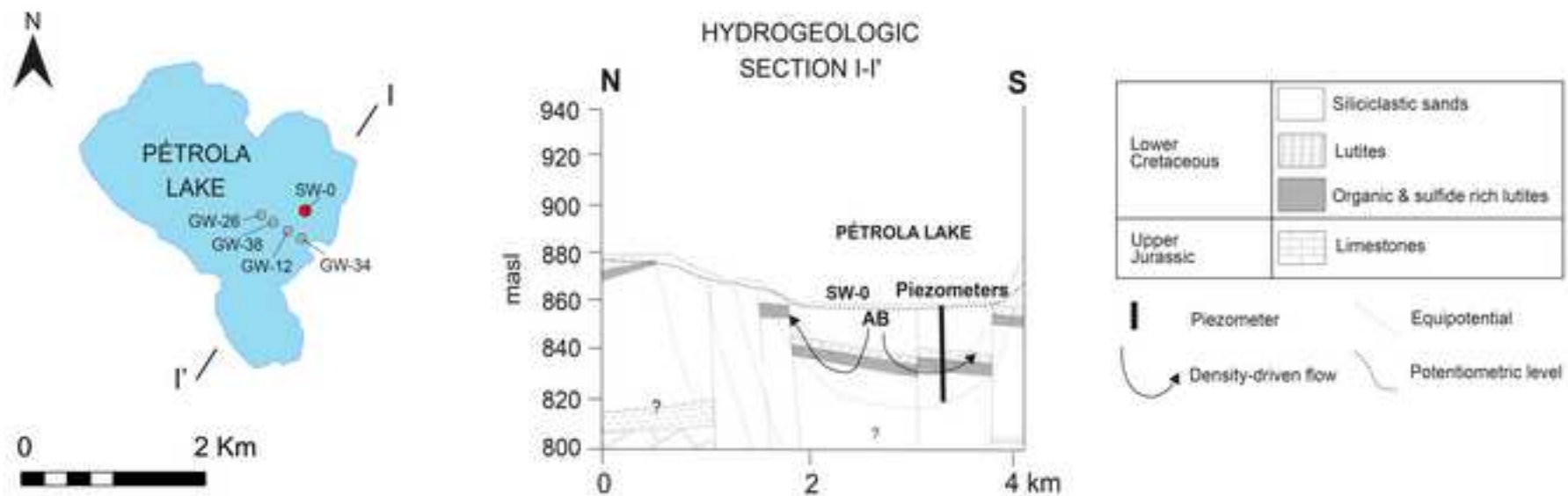
Figure3
[Click here to download high resolution image](#)
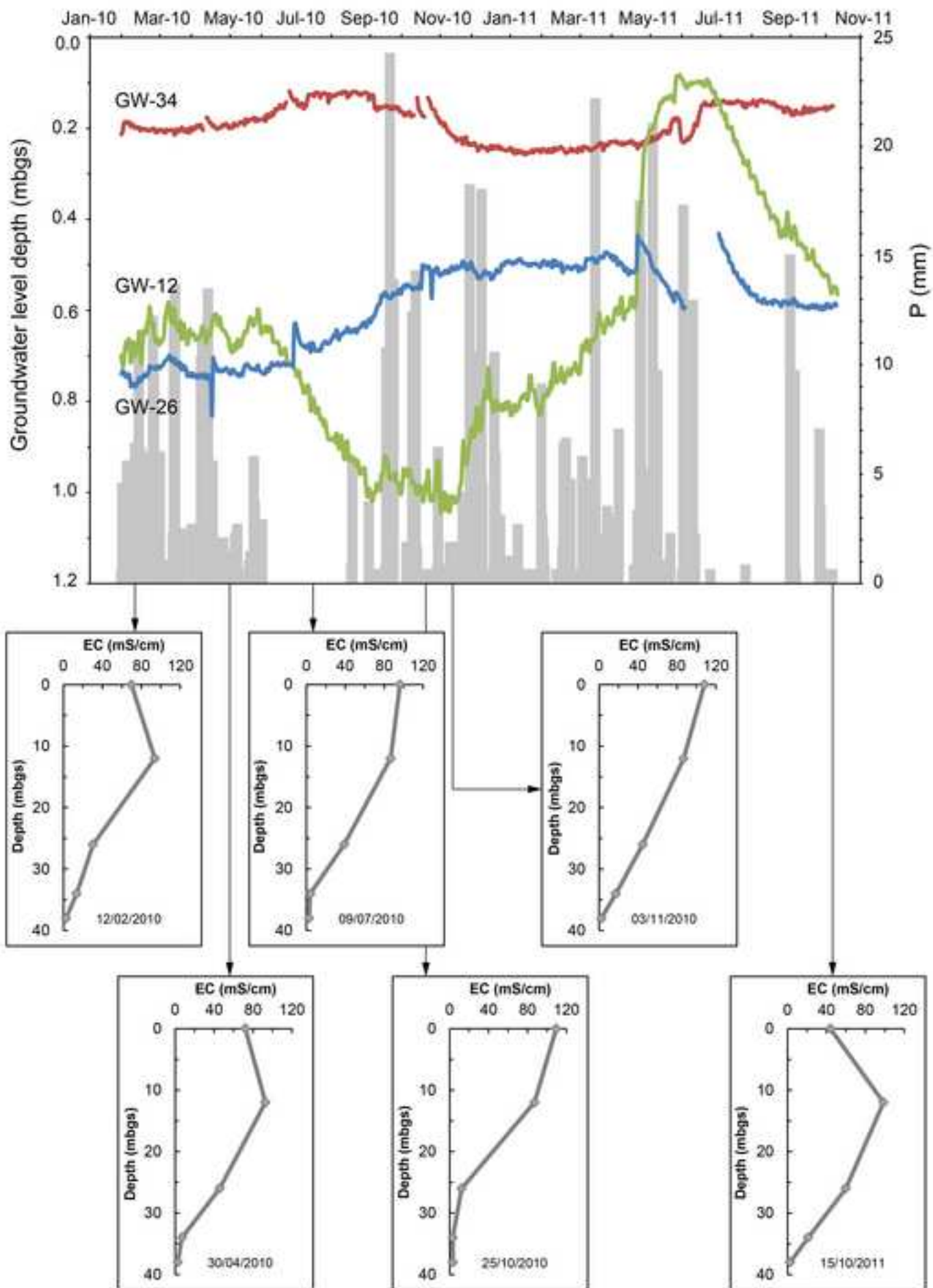
Figure4
Click here to download high resolution image
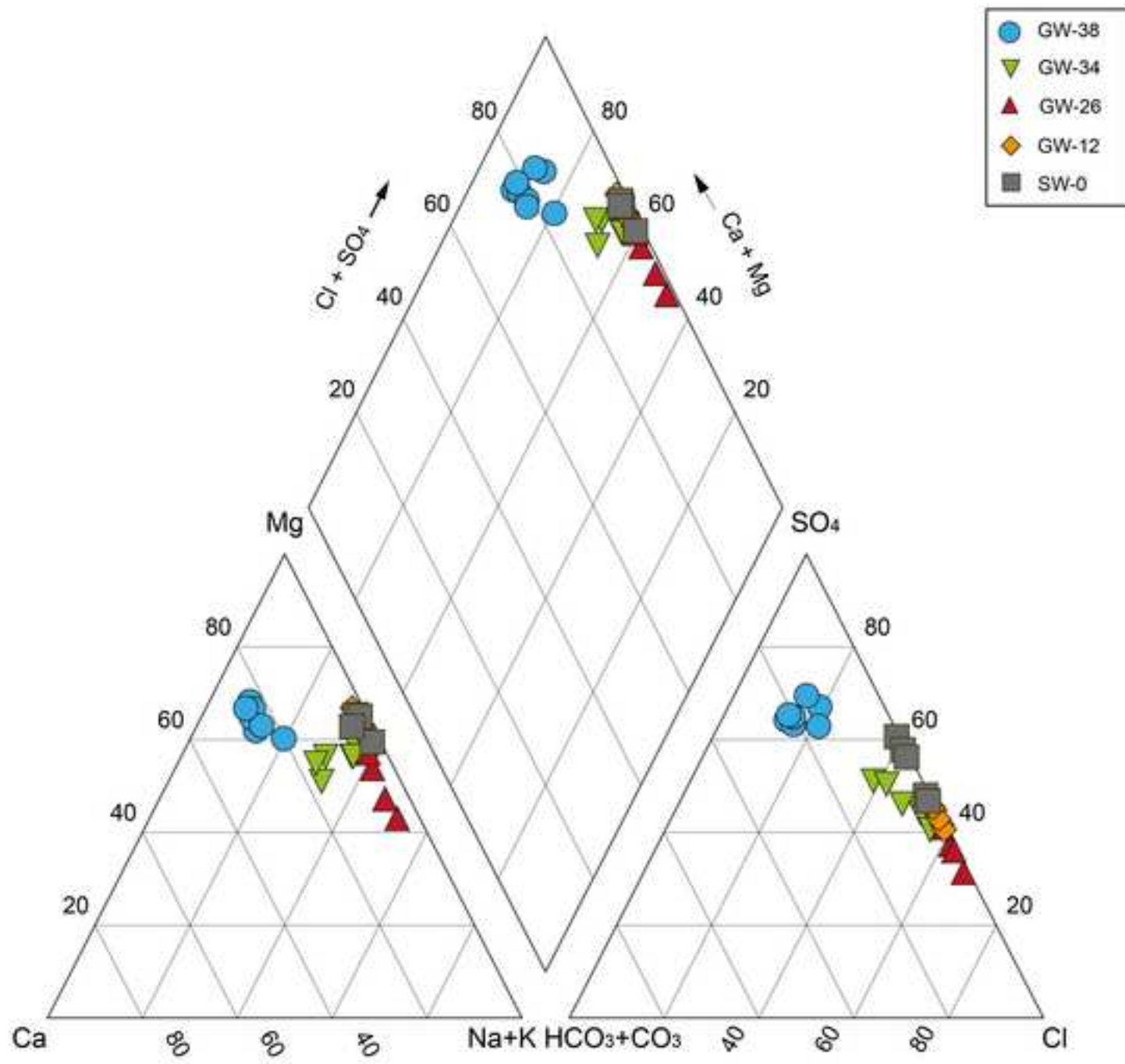
Figure5
Click here to download high resolution image

Figure 5. Plot of δ^2H [‰] versus $\delta^{18}O$ [‰] showing the Global Meteoric Water Line (GMWL: $\delta^2H = 8.1\ \delta^{18}O + 10.8$) and the Pétrola line ($\delta^2H = 5.2\ \delta^{18}O - 11.9$, $R^2 = 0.86$). Data points: GW-38, GW-34, GW-26, GW-12, SW-0, and WP.
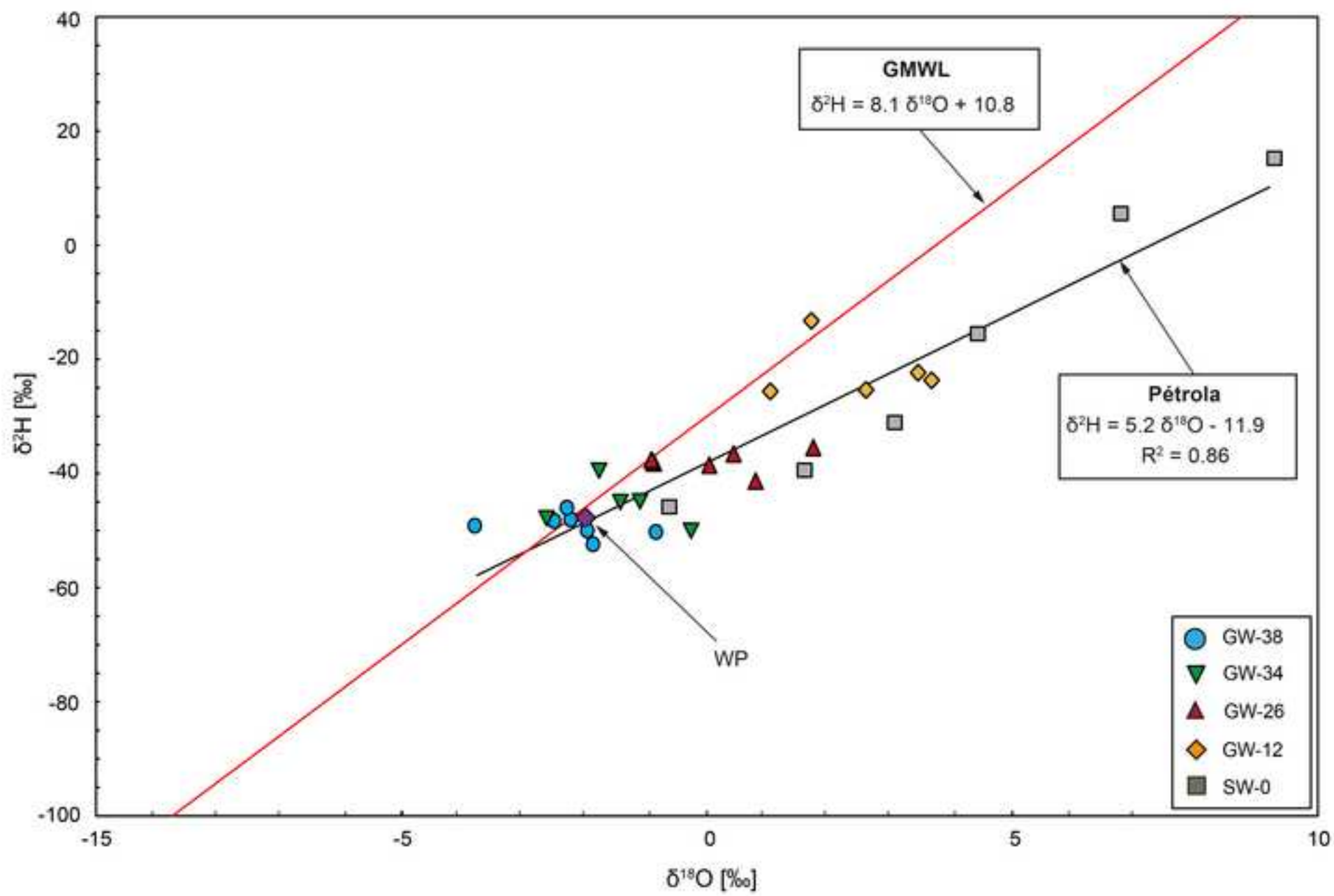
Figure6
Click here to download high resolution image
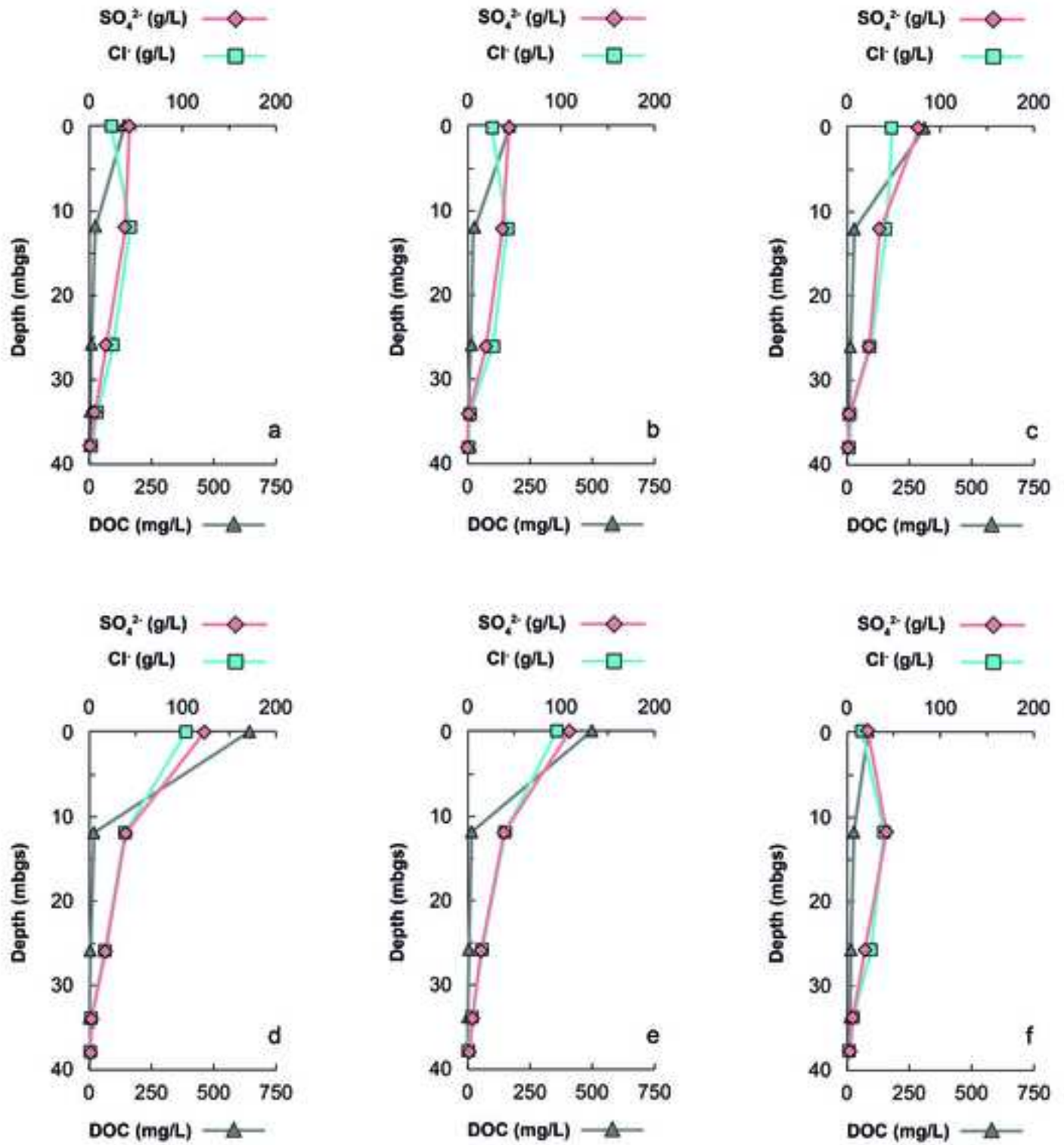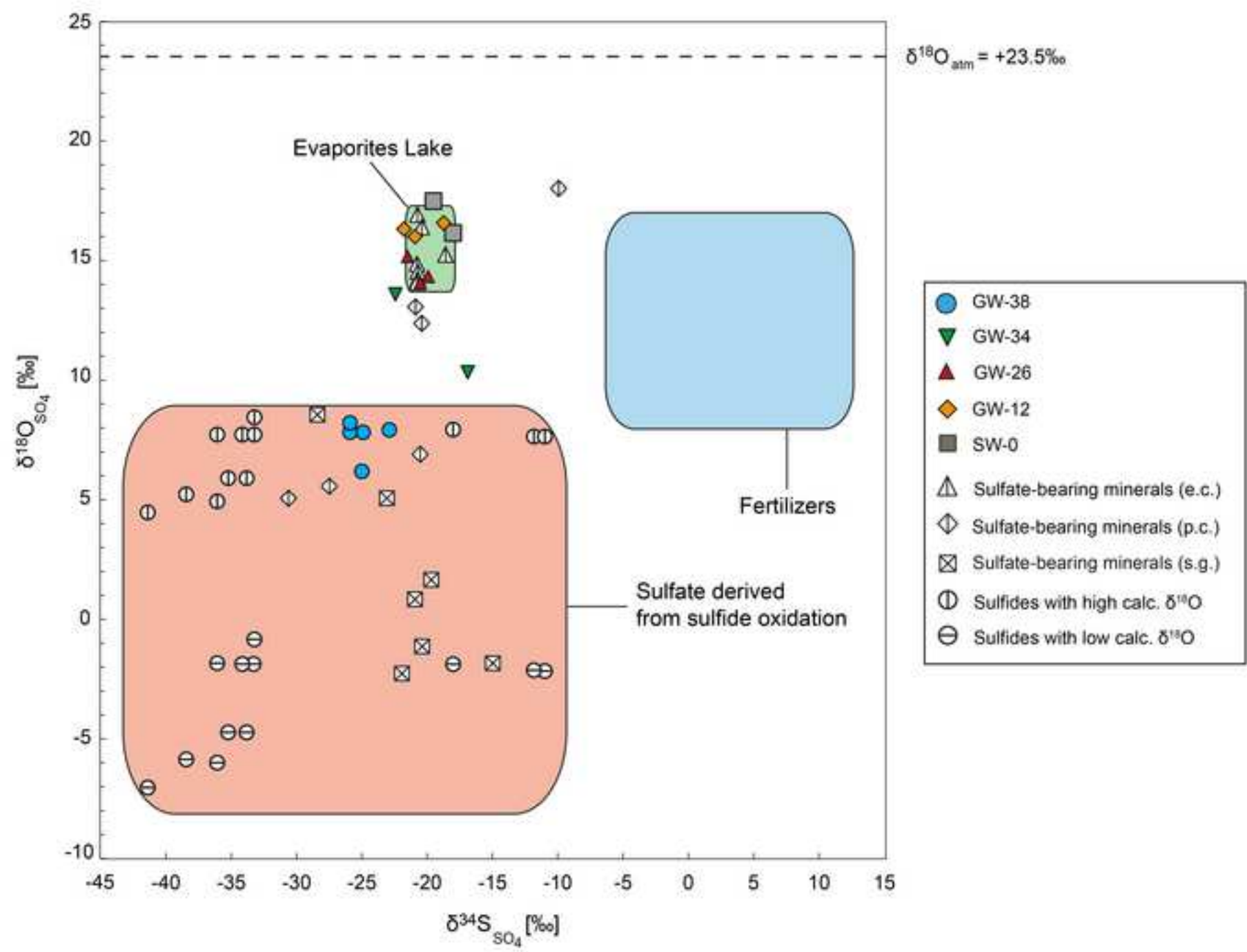
Figure8
Click here to download high resolution image
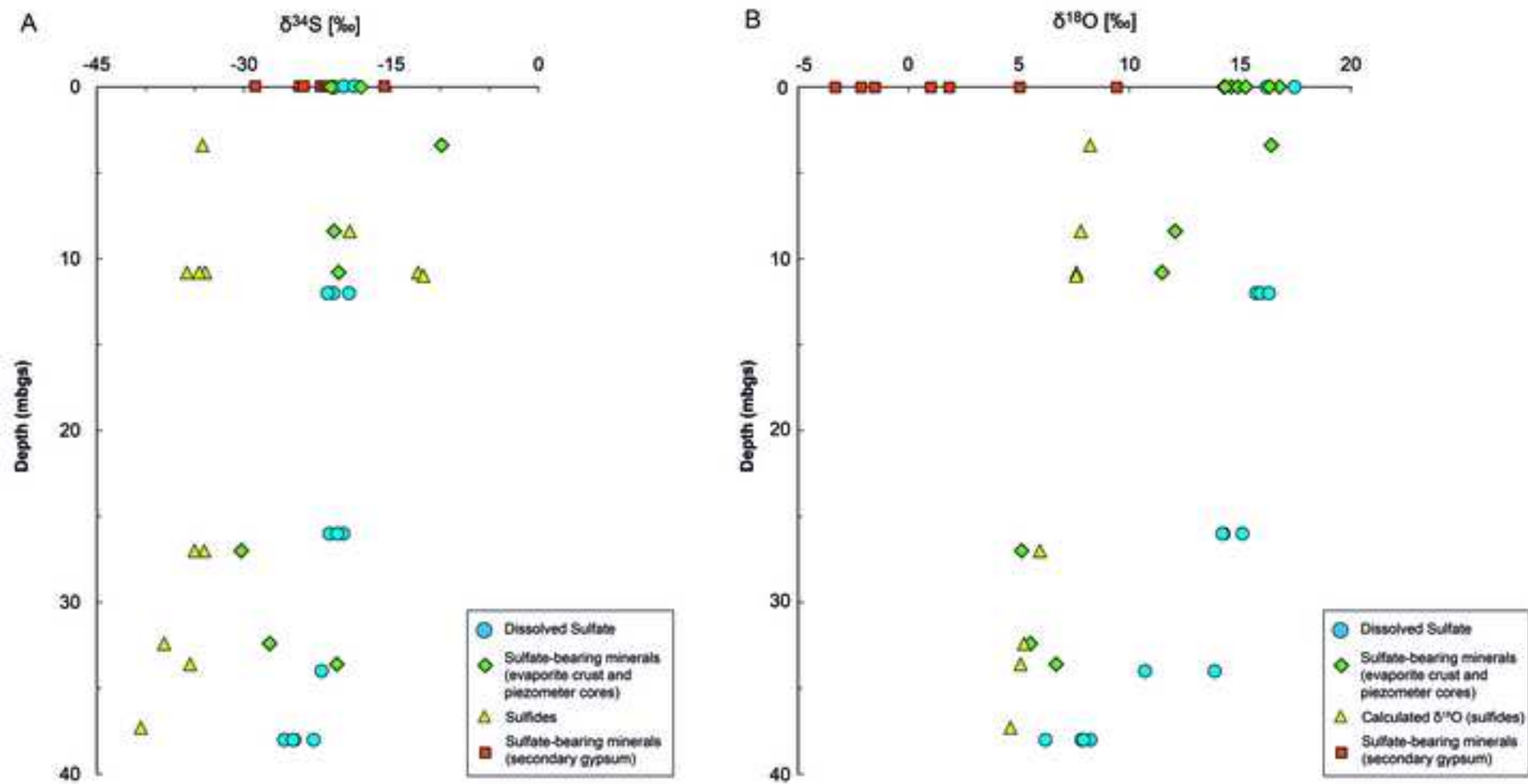
Figure9
Click here to download high resolution image

Tracing sulfate recycling in the hypersaline Pétrola Lake (SE Spain): A combined isotopic and microbiological approach

N. Valiente[a], R. Carrey[b], N. Otero[b,c], M.A. Gutiérrez-Villanueva[a], A. Soler[b], D. Sanz[a], S. Castaño[a], and J.J. Gómez-Alday[a]

a Biotechnology and Natural Resources Section, Institute for Regional Development (IDR), University of Castilla–La Mancha (UCLM), Campus Universitario s/n, 02071 Albacete, Spain

b Grup d'Mineralogia Aplicada i Medi Ambient, Dep. Mineralogia, Petrologia i Geologia Aplicada, Facultat de Ciències de la Terra, Universitat de Barcelona (UB), C/ Martí i Franquès s/n, 08028, Barcelona, Spain

c Serra Hunter Fellowship, Generalitat de Catalunya, Spain

Tables

Table 1. Tritium activity (TU) in water samples. GW: groundwater. SW: surface water.

Sample Point	Date	UT
GW-38	30/04/2010	0.8 ± 0.4
GW-34	30/04/2010	0.2 ± 0.4
GW-26	30/04/2010	0.9 ± 0.4
GW-12	18/06/2010	1.5 ± 0.3
SW-0	18/06/2010	4.6 ± 0.3

Table 2. Mean values for sample point of the chemical analyses in water samples (mg/L, except Fe and Mn in µg/L). EC: electric conductivity (µS/cm). Eh: redox potential (mV). DO: dissolved oxygen (mg/L). T: temperature (ºC). DOC: dissolved organic carbon (mg/L). BLD: below limit of detection. GW: groundwater. SW: surface water.

Sample Point	pH	EC	Eh	DO	T	SO_4	HCO_3	Cl	Na	K	Ca	Mg	Fe	Mn	DOC
GW-38	7.6	2,743.8	131.0	0.6	17.4	1,141.0	411.3	241.4	122.9	12.9	182.9	267.4	263.6	11.8	3.2
GW-34	7.0	11,068.3	95.7	0.4	18.9	3,538.2	465.4	3,283.6	1,438.7	134.3	287.3	1,186.4	BLD	0.2	3.2
GW-26	7.2	38,700.0	110.7	0.2	18.1	18,347.5	434.3	21,200.9	9,585.0	1,063.0	637.3	6,289.2	2.8	0.2	7.9
GW-12	7.1	90,983.3	3.0	1.3	18.4	38,115.8	475.8	39,618.7	15,483.3	2,685.0	444.9	14,200.4	3.1	0.2	21.1
SW-0	8.1	83,300.0	148.8	3.6	21.0	69,331.3	1,074.0	50,810.1	34,798.3	5,128.3	466.3	15,052.1	BLD	BLD	304.9

Table 3. Isotope values (‰) in water samples. GW: groundwater. SW: surface water. nd: no determined.

Sample Point	Date	$\delta^{34}S_{SO4}$	$\delta^{18}O_{SO4}$	δ^2H_{H2O}	$\delta^{18}O_{H2O}$
GW-38	10/09/2008	-24.9	+7.8	-50.2	-6.9
GW-38	09/12/2008	-25.9	+7.8	nd	nd
GW-38	15/05/2009	-25.9	+8.2	-48.5	-7.2
GW-38	12/02/2010	-22.9	+7.9	nd	-7.1
GW-38	30/04/2010	-25.0	+6.2	-50.5	-5.7
GW-38	09/07/2010	nd	nd	-46.6	-7.2
GW-38	25/10/2010	nd	nd	-52.4	-6.8
GW-38	03/11/2010	nd	nd	-48.7	-7.4
GW-38	15/10/2011	nd	nd	-49.5	-8.8
GW-34	12/02/2010	-22.1	+13.9	nd	-6.1
GW-34	30/04/2010	-16.2	+10.7	-49.9	-5.3
GW-34	09/07/2010	nd	nd	-45.0	-6.4
GW-34	25/10/2010	nd	nd	-44.8	-6.1
GW-34	03/11/2010	nd	nd	-39.6	-6.8
GW-34	15/10/2011	nd	nd	-47.7	-7.6
GW-26	15/05/2009	-19.9	+14.2	-38.7	-5.0
GW-26	12/02/2010	-21.3	+15.1	nd	-4.2
GW-26	30/04/2010	-20.5	+14.2	-35.9	-3.3
GW-26	09/07/2010	nd	nd	-36.9	-4.6
GW-26	25/10/2010	nd	nd	-41.2	-4.2
GW-26	03/11/2010	nd	nd	-38.3	-5.9
GW-26	15/10/2011	nd	nd	-37.8	-5.9
GW-12	15/05/2009	-20.9	+15.7	-22.3	-1.6
GW-12	12/02/2010	-21.5	+15.9	nd	-1.7
GW-12	30/04/2010	-19.3	+16.3	-23.5	-1.4
GW-12	09/07/2010	nd	nd	-25.1	-3.9
GW-12	25/10/2010	nd	nd	-24.9	-2.4
GW-12	03/11/2010	nd	nd	-14.5	-3.3
SW-0	26/02/2010	-20.0	+17.5	-45.1	-5.3
SW-0	30/04/2010	-18.9	+16.2	-15.5	-0.6
SW-0	09/07/2010	nd	nd	+15.1	+4.2
SW-0	25/10/2010	nd	nd	-30.2	-1.8
SW-0	03/11/2010	nd	nd	-39.1	-3.3
SW-0	15/10/2011	nd	nd	+6.8	+1.8

Table 4. Isotope values (‰) of $\delta^{34}S$ and $\delta^{18}O$ in S-bearing mineral samples. Depth in metres below ground surface (mbgs). nd: no determined.

Sample Point	Description	Mineral	Depth	$\delta^{34}S_i$	$\delta^{18}O_{SO4}$
ANNA-1	Core (GW-12)	Gypsum and hexahydrite	10.8	-20.3	+11.5
ANNA-17	Core (GW-34)	Gypsum and hexahydrite	33.6	-20.5	+6.7
ANNA-18	Core (GW-34)	Gypsum and hexahydrite	32.4	-27.4	+5.5
ANNA-20	Core (GW-38)	Gypsum and hexahydrite	27	-30.3	+5.1
ANNA-21	Core (GW-38)	Gypsum and hexahydrite	8.4	-20.8	+12.1
ANNA-22	Core (GW-38)	Gypsum and hexahydrite	3.4	-9.9	+16.4
PE MIN 1	Lake (SW-0)	Gypsum and hexahydrite	0	nd	+18.1
PE MIN 2	Lake (SW-0)	Gypsum and hexahydrite	0	nd	+18.2
PE MIN 3	Lake (SW-0)	Gypsum and hexahydrite	0	nd	+17.8
PE MIN 4	Lake (SW-0)	Gypsum and hexahydrite	0	nd	+17.5
PE MIN 5	Lake (SW-0)	Gypsum and hexahydrite	0	-20.5	+16.8
PE MIN 6	Lake (SW-0)	Gypsum and hexahydrite	0	-20.2	+16.3
PE MIN 7	Lake (SW-0)	Gypsum and hexahydrite	0	-20.5	+14.6
PE MIN 8	Lake (SW-0)	Gypsum and hexahydrite	0	-20.5	+14.3
PE MIN 9	Lake (SW-0)	Gypsum and hexahydrite	0	-20.5	+14.9
PE MIN 10	Lake (SW-0)	Gypsum and hexahydrite	0	-20.4	+14.3
PE MIN 11	Lake (SW-0)	Gypsum and hexahydrite	0	-18.3	+15.3
PE MIN 12	Lake (SW-0)	Gypsum and hexahydrite	0	nd	+17.1
PE ARMO 2	Utrillas Facies	Gypsum	0	-15.7	-1.8
PE ARMO 3	Utrillas Facies	Gypsum	0	-23.1	-2.8
PE ARMO 4 a	Utrillas Facies	Gypsum	0	-23.5	+5.1
PE ARMO 4 b	Utrillas Facies	Gypsum	0	-21.7	+1.1
PE ARMO 5	Utrillas Facies	Gypsum	0	-28.1	+9.0
PE ARMO 6	Utrillas Facies	Gypsum	0	-21.4	-1.1
PE ARMO 7	Utrillas Facies	Gypsum	0	-20.9	+2.3
ANNA-5	Core (GW-38)	Sulfide	27	-34.0	-
ANNA-7	Core (GW-12)	Sulfide	10.8	-35.8	-
ANNA-8	Core (GW-12)	Sulfide	10.8	-33.9	-
ANNA-10 b	Core (GW-12)	Sulfide	10.8	-34.6	-
ANNA-11 b	Core (GW-38)	Sulfide	10.8	-12.2	-
ANNA-12 b	Core (GW-38)	Sulfide	11	-11.7	-
ANNA-17 c	Core (GW-34)	Sulfide	33.6	-35.5	-
ANNA-18 c	Core (GW-34)	Sulfide	32.4	-38.1	-
ANNA-19 c	Core (GW-38)	Sulfide	37.3	-40.5	-
ANNA-20 c	Core (GW-38)	Sulfide	27	-35.0	-
ANNA-21 c	Core (GW-38)	Sulfide	8.4	-19.2	-
ANNA-22 c	Core (GW-38)	Sulfide	3.4	-34.2	-

Table 5. Mean saturation indices for gypsum, epsomite, halite, and hexahydrite. GW: groundwater. SW: surface water.

Sample Point	SI_{Gypsum}	$SI_{Epsomite}$	SI_{Halite}	$SI_{Hexahydrite}$
GW-38	-0.60	-2.88	-6.21	-3.23
GW-34	-0.38	-2.27	-4.23	-2.62
GW-26	0.03	-1.43	-2.52	-1.78
GW-12	-0.04	-0.97	-1.95	-1.30
SW-0	-0.03	-1.10	-1.60	-1.38

Supplementary Information - Appendix A

Supplementary Information - Appendix B

Supplementary Information - Appendix C